

---

# ATHEROMA PLAQUE VULNERABILITY BASED IN A 3D IDEALIZED PARAMETRIC GEOMETRY.

## MÁSTER MECÁNICA APLICADA

---

**Myriam Cilla Hernández**  
Ingeniero Industrial

---

*A todos los que me apoyan día a día...*

# ATHEROMA PLAQUE VULNERABILITY BASED IN A 3D IDEALIZED PARAMETRIC GEOMETRY.

---

## RESUMEN

Las enfermedades cardiovasculares constituyen la primera causa de mortalidad en los países desarrollados, así como en la práctica totalidad de los países en desarrollo [47]. Dentro de las patologías cardiovasculares, una de las enfermedades que más muertes causan hoy en día es la aterosclerosis. Dicha enfermedad consiste en la degeneración progresiva y crónica del engrosamiento y endurecimiento de la pared arterial como resultado de la acumulación de depósitos de grasa, colesterol y otras sustancias en la pared interna del vaso. Éstas sustancias forman estructuras duras llamadas placas de ateroma y en ellas se puede diferenciar diferentes composiciones; calcificación, lípidos y tejido fibroso. Con el tiempo, si estas placas son vulnerables pueden romperse y provocar la formación de coágulos sanguíneos que bloquean el flujo sanguíneo desencadenando diferentes eventos tales como infartos, trombos o gangrena [1, 58]. La importancia de identificar la placa vulnerable antes de su rotura sigue siendo un reto para la medicina. Actualmente el diagnóstico se puede realizar por métodos no invasivos, tales como es determinar la presencia de factores de riesgo, marcadores de vulnerabilidad de la placa, y métodos invasivos como es la angioscopia. Aunque existen varios métodos, no existe uno que nos de toda la información morfológica y de actividad de la placa necesaria.

El objetivo principal de este trabajo es el estudio y modelado de vasos sanguíneos, concretamente de una coronaria, afectados por aterosclerosis. Para ello, se ha desarrollado un estudio paramétrico en tres dimensiones (3D) de los factores geométricos en la vulnerabilidad de la placa de ateroma y de la influencia de las tensiones residuales. Los modelos en 3D nos permiten incluir los efectos producidos por las tensiones residuales. Con dichos modelos se van a estudiar tres situaciones diferentes; sin tensiones residuales, considerando tensiones residuales en dirección longitudinal y por último, considerando tensiones residuales tanto en dirección longitudinal como circunferencial. De este modo, se podrá identificar el papel que juegan las tensiones residuales en la vulnerabilidad de la placa de ateroma y definir límites de vulnerabilidad para cada uno de los parámetros considerados. Los modelos se han simulado mediante elementos finitos con el software comercial ABAQUS. Los resultados obtenidos, nos permiten ir un paso más allá en el diagnóstico preventivo y en la planificación preoperatoria en aplicaciones cardiovasculares.

Con el fin de validar el modelo, se ha reconstruido mediante el software comercial MIMICS una geometría real a partir de un IVUS (ultrasonido intravascular) de un paciente adulto con placa de ateroma. Tras la reconstrucción se han medido los parámetros estudiados en la geometría real y la hemos comparado con el correspondiente caso paramétrico de parámetros similares.



# Contents

<b>1</b>	<b>INTRODUCTION</b>	<b>1</b>
1.1	Cardiovascular diseases . . . . .	1
1.1.1	Atherosclerosis . . . . .	1
1.2	Physiology and properties of the blood vessels . . . . .	3
1.2.1	Layers . . . . .	3
1.2.2	Residual stresses . . . . .	4
1.3	Constitutive modelling of anisotropic material . . . . .	4
1.3.1	Hyperelastic model . . . . .	5
1.3.2	Strain energy functions . . . . .	6
1.4	Objectives and motivation . . . . .	7
1.5	Contents . . . . .	8
<b>2</b>	<b>3D PARAMETRIC STUDY</b>	<b>9</b>
2.1	Modeling of the atherosclerotic coronary artery . . . . .	9
2.1.1	Idealized geometry . . . . .	9
2.1.2	Parameters studied . . . . .	10
2.1.3	Mesh . . . . .	11
2.1.4	Material properties . . . . .	12
2.1.5	Boundary conditions . . . . .	14
2.2	Results . . . . .	15
2.2.1	Statistical Analysis . . . . .	15
2.2.2	Trend analysis . . . . .	18
2.2.3	Vulnerability study . . . . .	19
2.2.4	Vulnerability factor . . . . .	23
2.3	Importance of 3D models . . . . .	25
<b>3</b>	<b>REAL GEOMETRY VERSUS IDEALIZED GEOMETRY</b>	<b>27</b>

<b>4 CONCLUSIONS AND FUTURE WORK</b>	<b>30</b>
4.1 Conclusions . . . . .	30
4.2 Limitations . . . . .	33
4.3 Future work . . . . .	34

# INTRODUCTION

## 1.1 Cardiovascular diseases

Cardiovascular diseases (CVD) are nowadays primary causes of mortality in the developed world and it has been calculated that they will become the first cause of death worldwide in 2020 [40]. Cardiovascular disease is divided into several categories of subclasses. The most important one, in terms of annual deaths, is Coronary Heart Disease (CHD), also referred to as Coronary Artery Disease (CAD), which refers to the disease of the blood vessels supplying the heart muscle [1, 44, 54].

Due to the huge social and economical impact of CVDs, the study of the blood vessel and their associated pathologies have been one of the main research topics in medicine in the last decades. More recently, the mechanical factors influencing the vascular pathologies have been considered in Biomechanics [19]. Specifically, arteries have been focused most of the efforts due to their higher tendency to develop disease pathologies, whereas veins have not been so deeply studied. The studies developed until the date demonstrate that mechanics play a determinant role in the development and evolution of a variety of pathologies [31], which itself justifies the thorough investigation of their mechanical response both in healthy and diseased states.

### 1.1.1 Atherosclerosis

The main dominant cardiovascular disease is arteriosclerosis, which is the process in which plaques - consisting of deposits of cholesterol and other lipids, calcium and large inflammatory cells called macrophages - are built up in the walls of the arteries causing narrowing (stenosis of the lumen), hardening of the arteries and loss of their elasticity, which leads to a reduction in the blood flow through the vessels. Nevertheless, the most serious damage occurs when the plaque becomes fragile and ruptures (vulnerable plaque). Plaque rupture

causes the formation of blood clots that can block blood flow or break off and travel to another part of the circular system thus producing heart attacks, strokes, difficulty in walking and eventually gangrene [25, 36, 62], see Figure 1.1.

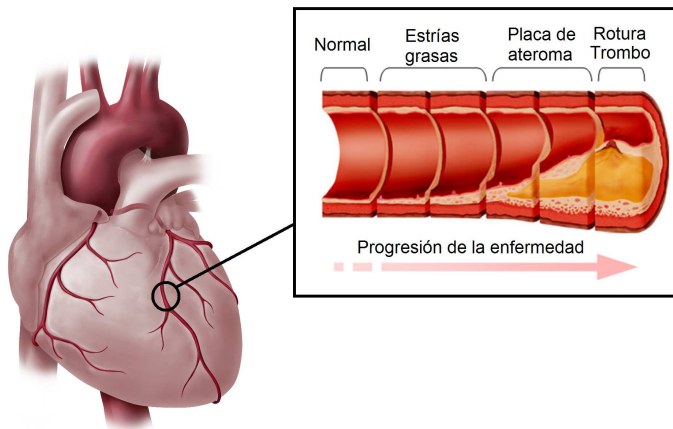


Figure 1.1: Coronary artery atherosclerosis.

Until now, several methods have been used to evaluate the extent and location of atherosclerotic lesions; invasive methods such as IVUS (intravascular ultrasound) or X-ray angiography and non-invasive methods, which detect indicators of atherosclerosis such as classical risk factors [16, 33, 38]. Identifying vulnerable patients before plaque rupture occurs would help clinicians to provide early treatment as well as to take preventive measures. Many strategies have been proposed to achieve this goal, though available screening and diagnostic methods seem to be insufficient.

The characteristics of vulnerable plaque have been well defined in several pathological studies [20, 55, 46, 64, 68] amongst others. Plaque rupture is believed to be related to plaque morphology, mechanical forces, vessel remodelling, blood conditions (levels of cholesterol, sugar, etc.), chemical environment and lumen surface conditions (inflammation) [63]. Regarding the mechanical forces, some authors [49, 67] consider the peak circumferential stress (PCS) as the most important biomechanical factor in the mechanisms leading to rupture of the atherosclerotic plaque, and have often used it as a predictor of atherosclerotic plaque rupture location. Previous works have shown that reduced fibrous cap thickness increases the maximal value of the PCS exponentially, and leads the cap stress to exceed the rupture threshold of 300 kPa [10, 39, 49] when the cap thickness becomes lower than 65  $\mu\text{m}$  [17, 45, 66, 68].

The fibrous cap thickness has typically been identified as the key predictor of vulnerability and likelihood of rupture, but some clinical and biomechanical studies have shown that this single parameter is not a reliable predictor of plaque stability [35, 69], since

plaque stability also depends on other intrinsic properties of the plaque, such as the size and the consistency of the soft atheroma core [17, 21], the cap and the core inflammation levels [4, 37] and the arterial remodelling index, which is defined as the external elastic membrane area at plaque divided by the external elastic membrane area at a nearest segment judged to be free of plaque. [48, 57, 65].

## 1.2 Physiology and properties of the blood vessels

### 1.2.1 Layers

The blood vessels are made of a layered structure which, when healthy, is usually composed of three different *tunicas* or layers. From the inner to the outer radius, they are the intima, the media, and the adventitia, whose main features are the following, (see Figure 1.2).

- **Intima:** The intimal layer is the innermost layer of all blood vessels, being composed of the following structures: 1) a single layer of endothelial cells lining the vascular wall; 2) a thin, about 80 [nm] thick, elastic lamina; and 3) a subendothelial layer, composed of collagenous bundles, elastic fibrils, smooth muscle cells, and perhaps some fibroblasts. The subendothelial layer, however, is only presented in large elastic arteries such as the human aorta, whereas this sub-layer is missing in other smaller arteries.
- **Media:** The tunica media, as the name indicates, is the middle layer of the vascular wall. It is made of smooth muscle cells, a variable number of elastic laminae, bundles of collagenous fibrils and a network of elastic fibrils. This layer is thicker in arteries than in veins, in which muscle cells may be absent in large veins like vena cava. In the aorta, the media layer may reach thicknesses of 500 [ $\mu\text{m}$ ], whereas is about 20-50 [ $\mu\text{m}$ ] in medium sized veins.
- **Adventitia:** The tunica adventitia is the outermost layer of the vascular wall. Its thickness varies considerably depending on the type and location of the blood vessel. In all arteries, and most veins, the adventitia consists of dense fibroelastic tissue without smooth muscle cells, except in large veins, such as vena cava, where bundles of longitudinally arranged smooth muscle cells may be found. Also the nutrient vessels of the vascular wall that take nutrients to the muscle cells in the media, namely the *vasa vasorum*, are part of the adventitia, as well as nerves. The adventitia renders the vascular wall a fair amount of stability, and serves to connect blood vessels to the surrounding tissue.

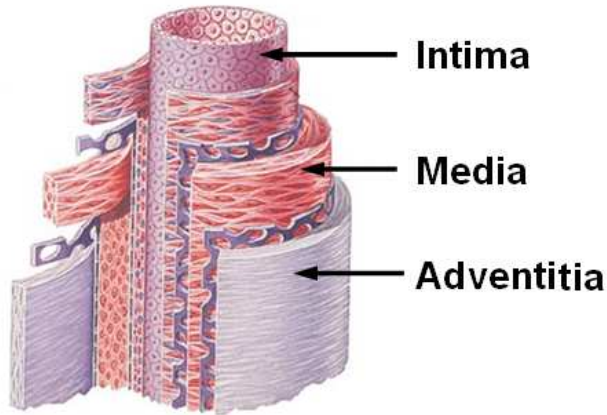


Figure 1.2: Representation of the arterial wall and its layers; intima, media and adventitia

### 1.2.2 Residual stresses

The presence of residual stresses in the blood vessels wall is one of the most important features of vascular tissues. Residual stresses are defined as those stresses present in the vessels when no loads are applied, and are revealed when a cut is performed on a vessel in an unloaded configuration. Then, considering a cut in the radial direction, the vessel shortens (or lengthens) releasing part of the residual stresses in the longitudinal direction. Also when a cut is performed in the longitudinal direction, usually on a short vessel ring, it springs open releasing the residual stress associated to the circumferential direction.

With these considerations at hand, the inclusion of residual stresses in blood vessels models is of crucial importance for their accurate mechanical modelling.

## 1.3 Constitutive modelling of anisotropic material

In the context of mathematical modelling and finite element simulation, the experimental data are used to estimate the material model parameters through a strain energy function (SEF) within the framework of the continuum theory of large deformation hyperelasticity.

In order to define the mathematically model of the tissue behaviour (blood vessel wall, atheroma plaque and lipid core) several considerations should be taken account. Firstly, the tissue samples experienced finite strains for small loads. Secondly, a strongly marked nonlinearity was found. Thirdly, there is a remarkable anisotropy behaviour in the tissue belong to the blood vessel wall. Thus, a preferential direction of anisotropy is considered, through the angle  $\alpha$  referred to the circumferential direction, Figure 2.3. Atheroma plaque and lipid core tissue are considered as isotropic materials.

### 1.3.1 Hyperelastic model

A common way to formulate an elastic constitutive law under isothermal conditions for fibred soft tissues, [29, 53, 70], is to postulate the existence of a SEF that depends on the direction of the family of fibres at a point  $\mathbf{X}$  that is defined by the unit vector field  $\mathbf{m}_0$  [58]. The stretch  $\lambda_m$  of the fibres defined as the ratio between its lengths at the deformed and reference configurations is:

$$\lambda_m^2 = \mathbf{m}_0 \cdot \mathbf{C} \mathbf{m}_0 \quad (1.1)$$

where  $\mathbf{F} = \frac{\partial \mathbf{x}}{\partial \mathbf{X}}$  and  $\mathbf{C} = \mathbf{F}^T \mathbf{F}$  are the standard deformation gradient and the corresponding right Cauchy-Green strain measure, respectively.

In order to handle more easily the quasi-incompressibility constraint, a multiplicative decomposition of  $\mathbf{F} = J^{\frac{1}{3}} \bar{\mathbf{F}}$  and  $\mathbf{C} = J^{\frac{2}{3}} \bar{\mathbf{C}}$  into volume-changing and volume-preserving parts is usually established, as in Simo [56], where  $J$  is the Jacobian.

To characterize isothermal processes, it is postulated the existence of a unique decoupled representation of the strain-energy density function  $\Psi$ :

$$\Psi(\mathbf{C}, \mathbf{M}, \mathbf{N}) = \Psi_{vol}(J) + \bar{\Psi}(\bar{\mathbf{C}}, \mathbf{M}, \mathbf{N}) \quad (1.2)$$

where  $\Psi_{vol}(J)$  and  $\bar{\Psi}_{passive}$  are given scalar-valued functions of  $J$  and  $\bar{\mathbf{C}}$ ,  $\mathbf{M} = \mathbf{m}_0 \otimes \mathbf{m}_0$  and  $\bar{\mathbf{C}}$ ,  $\mathbf{N} = \mathbf{n}_0 \otimes \mathbf{n}_0$ , respectively, that describe the volumetric and isochoric responses of the material [27, 70]. This isochoric response is also formed by the active and passive response of the material;  $\mathbf{M}$  and  $\mathbf{N}$  are the preferential direction of anisotropy for the collagen fibers and muscle fibers, respectively.  $\bar{I}_1$  and  $\bar{I}_2$  are the first and second modified strain invariants of the symmetric modified Cauchy-Green tensor  $\bar{\mathbf{C}}$ . Finally, the invariants  $\bar{I}_4 \geq 1$  and  $\bar{I}_6 \geq 1$  characterizes the constitutive response of the fibres in the passive and active behaviour, respectively:

$$\bar{I}_4 = \bar{\mathbf{C}} : \mathbf{M} = \bar{\lambda}_m^2 \quad (1.3)$$

$$\bar{I}_6 = \bar{\mathbf{C}} : \mathbf{N} = \bar{\lambda}_n^2 \quad (1.4)$$

The constitutive equation for quasi-compressible hyperelastic materials can be defined from the Clausius-Planck inequality as:

$$\mathbf{S} = 2 \frac{\partial \Psi(\mathbf{C}, \mathbf{M}, \mathbf{N})}{\partial \mathbf{C}} = \mathbf{S}_{vol} + \bar{\mathbf{S}} = J p \mathbf{C}^{-1} + 2 \frac{\partial \bar{\Psi}(\bar{\mathbf{C}}, \mathbf{M})}{\partial \mathbf{C}} \quad (1.5)$$

where the second Piola-Kirchhoff stress  $\mathbf{S}$  consists of a purely volumetric contribution  $\mathbf{S}_{vol}$  and a purely isochoric one  $\bar{\mathbf{S}}$ ; being  $p = \frac{d\Psi_{vol}(J)}{dJ}$  the hydrostatic pressure. The Cauchy stress tensor  $\boldsymbol{\sigma}$  is  $1/J$  times the push-forward of  $\mathbf{S}$  ( $\boldsymbol{\sigma} = J^{-1} \chi_*(\mathbf{S})$ ) [27].

Knowing the second Piola-Kirchhoff stress  $\mathbf{S}$ , the elastic tensor  $\mathbf{C}$  is defined in the

material configuration as follows:

$$\mathbb{C} = 2 \frac{\partial \mathbf{S}(\mathbf{C}, \mathbf{M}, \mathbf{N})}{\partial \mathbf{C}} \quad (1.6)$$

The elastic tensor  $\mathbb{C}$  consists of a purely volumetric contribution and a purely isochoric response [27]:

$$\mathbb{C} = \mathbb{C}_{vol} + \bar{\mathbb{C}} = 2 \frac{\partial \mathbf{S}_{vol}}{\partial \mathbf{C}} + 2 \frac{\partial \bar{\mathbf{S}}}{\partial \mathbf{C}} \quad (1.7)$$

The elastic tensor in the spatial configuration, denoted by  $\mathbb{C}$ , is  $1/J$  times the push-forward of  $\mathbb{C}$  ( $\mathbb{C} = J^{-1} \chi_*(\mathbb{C})$ ) [27].

### 1.3.2 Strain energy functions

Within the framework of hyperelasticity, a brief review of the constitutive laws frequently used for modelling the passive behaviour of soft biological tissues, in particular of the vascular tissue, is presented in this section.

A model including two directions of anisotropy, specifically designed for the arterial tissue was developed by Holzapfel [27]. An exponential behaviour to represent the collagen fibres contribution, which was only considered under tension, was chosen, i.e.

$$\begin{aligned} \bar{\Psi}(\mathbf{C}, \mathbf{M}, \mathbf{N}) &= \mu [\bar{I}_1 - 3] + \frac{k_1}{2k_2} \left[ \exp \left( k_2 [\bar{I}_4 - 1]^2 \right) - 1 \right] \\ &+ \frac{k_3}{2k_4} \left[ \exp \left( k_4 [\bar{I}_6 - 1]^2 \right) - 1 \right], \end{aligned} \quad (1.8)$$

where the neo-Hookean term is associated to the ground substance with constant  $\mu$ , and the parameters  $k_1$  and  $k_3$  are stress-like, whereas  $k_2$  and  $k_4$  are dimensionless. As its main contribution, it is worth remarking that the directions of anisotropy were helically distributed, with an orientation angle of  $\pm\vartheta$  degrees with respect to the circumferential direction. This assumption is an attempt to mimic the real fibre distribution.

In order to include certain amount of fibre dispersion around the anisotropy directions characterized by the invariants  $I_4$  and  $I_6$ , Holzapfel's model was modified in Holzapfel et al. [28], where the functional

$$\begin{aligned} \bar{\Psi}(\mathbf{C}, \mathbf{M}, \mathbf{N}) &= \mu [\bar{I}_1 - 3] \\ &+ \frac{k_1}{k_2} \left[ \exp \left( k_2 \left[ [1 - \rho] [\bar{I}_1 - 3]^2 + \rho [\bar{I}_4 - 1]^2 \right] \right) - 1 \right] \\ &+ \frac{k_3}{k_4} \left[ \exp \left( k_4 \left[ [1 - \rho] [\bar{I}_1 - 3]^2 + \rho [\bar{I}_6 - 1]^2 \right] \right) - 1 \right], \end{aligned} \quad (1.9)$$

was proposed. This expression includes the exponential dependence on the factor  $[\bar{I}_1 - 3]$  as well as the dimensionless weighting parameter  $\rho \in [0, 1]$ . By means of this parame-

ter, which has a purely phenomenological basis, it is possible to regulate the degree of anisotropy.

With the same spirit, Gasser et al. [22] proposed the strain energy density function

$$\begin{aligned}\bar{\Psi}(\mathbf{C}, \mathbf{M}, \mathbf{N}) = & \mu [\bar{I}_1 - 3] \\ & + \frac{k_1}{2k_2} \left[ \exp \left( k_2 [\kappa \bar{I}_1 + [1 - 3\kappa] \bar{I}_4 - 1]^2 \right) - 1 \right] \\ & + \frac{k_3}{2k_4} \left[ \exp \left( k_4 [\kappa \bar{I}_1 + [1 - 3\kappa] \bar{I}_6 - 1]^2 \right) - 1 \right],\end{aligned}\quad (1.10)$$

where  $\kappa \in [0, 1/3]$  is a measure of the dispersion around the preferred orientations determined by  $\bar{I}_4$  and  $\bar{I}_6$ . However, contrary to the expression in (1.9) where  $\rho$  basically couples the invariants  $\bar{I}_1$  and  $\bar{I}_4$  (or  $\bar{I}_1$  and  $\bar{I}_6$ ), a structurally consistent derivation where the structural components of the vessel wall are reflected by associated entities in the formulation leads to the derivation of  $\kappa$ . Specifically, this parameter is a result of considering the fibres oriented following the von Mises orientation density function. Thus, isotropy is reached for  $\kappa = 1/3$ , whereas  $\kappa = 0$  renders no fibre dispersion.

## 1.4 Objectives and motivation

The main objective of the present work is to advance towards the develop of a numerical and experimental methodology for modelling a vascular pathologies such as the atherosclerosis.

In this context, the goal of this study is to present a 3D parametric study of the geometric risk factors in an idealized coronary vessel to quantify and investigate the biomechanical interaction between the most influential values of the geometry of the vessel in the plaque rupture: (i) the fibrous cap thickness; (ii) the stenosis ratio; (iii) the lipid core width and (iv) the lipid core length. Furthermore, the influence of residual stresses on the risk of atheroma plaque has been shown by comparing three set of idealized 3D geometries incorporating residual stresses (one set taking account just the longitudinal RS and other with the longitudinal and the circumferential RS included) and without them.

Several parametric studies have been performed in two dimensions (2D) assuming the plane strain hypothesis in order to study the mechanical risk factor of vulnerable plaque [10, 37, 17, 49, 48]. Nevertheless, some of this studies show that a 2D structural analysis tends to overestimate the amplitude of the PCS [49]. In addition, longitudinal residual stress effects and other features such as the anisotropy or the longitudinal length of the plaque can not be considered in 2D models.

Thus, there is a need for a parametric 3D study to analyze the influence of the most influential geometric parameters on the biomechanical stability of vulnerable coronary plaques and assess the role of circumferential and axial residual stresses. The performed

3D studies related to the atheroma plaque are usually carried out on geometries obtained from IVUS or MRI (Magnetic Resonance Imaging) [5, 8, 49] and residual stresses are neglected. And, even though the performance and importance of 3D models has been demonstrated to identify vulnerable plaques [11, 49], no idealized and parametric 3D studies have attempted to this purpose.

## 1.5 Contents

Chapter 1 includes a introduction of the cardiovascular diseases and its impact in our society. Besides, the constitutive modelling of anisotropic material models is shown. Next, the objectives of this work are listed and, finally, their contents are described.

Chapter 2 includes the description and results of the 3D parametric model performed in order to help clinicians to fully understand the mechanical factors which promote plaque rupture. Also, the influence of residual stress on the stability of vulnerable coronary plaques have been shown by comparing three set of idealized 3D geometries incorporating residual stress (one set taking into account just the longitudinal residual stress and other with the longitudinal and circumferential residual stress included) and without them. Also, the results obtained in the parametric study are included in this chapter. Furthermore, a comparison between the results obtained by the 3D model used in this parametric study with the plane strain model usually employed in the literature to study the vulnerability of the plaque have been carried out in order to show the accuracy of plane strain models up.

Chapter 3 includes the validation of the idealized geometry of the atherosclerotic artery used in the 3D parametric study by a patient-specific coronary vessel geometry reconstruction. The results obtained in the real reconstructed vessel and in the idealized model have been compared.

Finally, Chapter 4 resume the main conclusions obtained from this project, describes some limitations of the study and proposes some future lines of work in order to improve that investigation.

# Chapter 2

## 3D PARAMETRIC STUDY

### 2.1 Modeling of the atherosclerotic coronary artery

#### 2.1.1 Idealized geometry

A 3D parametric study of the influence of the geometric factors was performed to check the vulnerability of the atherosclerotic plaque. For this purpose, a 3D finite element model was developed in the commercial finite element code ABAQUS 6.9, taking into account both the composition and the dimensions of the different layers of the tissue (media and adventitia), the fibrous plaque and the lipid core.

An idealized geometry corresponding to a coronary vessel with a eccentric atheroma plaque was modelled. The plaques was characterized by a large lipid pool with a thin fibrous cap [13, 17, 50]. Atherosclerotic vessel morphology and average dimensions were obtained from Versluis et al. [67] and Bluestein et al. [7]. A vessel length of 20 mm, a external radius of 2 mm and a vessel wall thickness of 0.5 mm were considered to create the basic geometry.

The arterial wall was assumed as a hollow cylinder and the lumen was consider circular. The atherosclerotic plaque, which is located inside the vessel, was assumed to be symmetric with respect to the central cross section. Finally, the lipid core was approximated as a blunt volume. In areas with atheroma plaque, the whole media layer was considered as fibrotic, whereas only the adventitia was considered to be a healthy layer. Figure 2.1.a shows the transversal section of the atherosclerotic coronary vessel described and the main parts of the model considered; wall vessel composed by the adventitia and the media layers, lipid core and atheroma plaque.

### 2.1.2 Parameters studied

The parametric model consists of a series of idealized plaque morphology models, mimicking different stages and variations of the atherosclerotic lesion growth. Previous analyses were first performed on the model in order to identify the most influential geometric parameters on the atheroma vulnerability risk. Geometric parameters such as the lipid core angle were rule out as one of the most influential parameters.

Following the results of these previous test and several works of the literature [10, 17, 48, 72], the most influential geometric parameters considered were the fibrous cap thickness ( $fc$ ), the stenosis ratio ( $sr$ ) - which is obtained by dividing the lumen radius by the lumen radius of a normal artery ( $R = 1.5$  mm),  $sr(\%) = \frac{r(\text{mm})}{R(\text{mm})} 100$  - the lipid core length ( $l$ ) and the lipid core width ( $w$ ). The lipid core width ( $w$ ) was defined as the ratio between the percentage of the atheroma plaque width ( $w_1$ ) and the distance from the inner point of the lipid core to the outer point of the fibrotic plaque ( $w_2$ ),  $w(\%) = \frac{w_1(\text{mm})}{w_2(\text{mm})} 100$ . The cross central section of the 3D model with the parameter studied marked is shown in Figure 2.1.b, where the lipid core length was measured along the longitudinal direction (Figure 2.1.a).

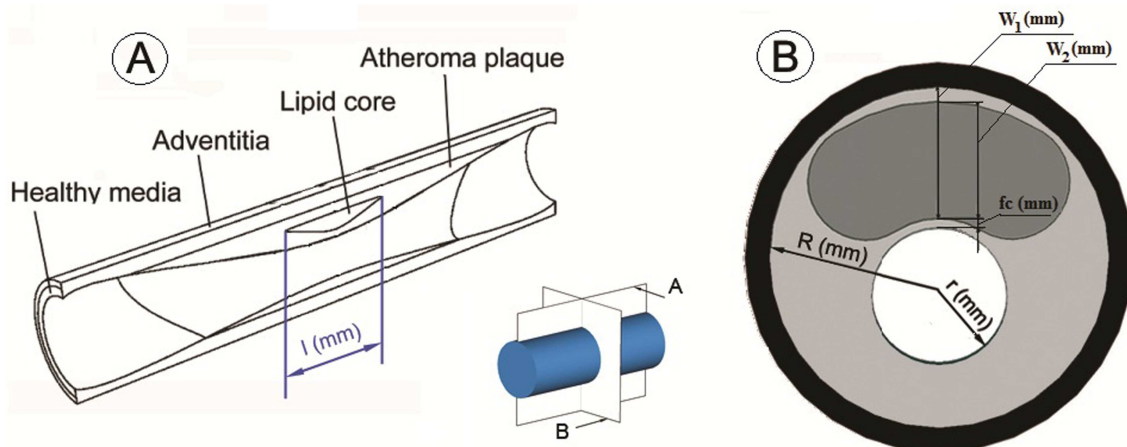


Figure 2.1: (A) Idealized geometry of an atherosclerotic arterial model. Transversal section. (B) Geometrical parameters shown on the cross central section of the atherosclerotic vessel.

Five values for each parameter were considered and combined which makes a total of  $625 = 5^4$  idealized eccentric vessel models with atherosclerotic lesions. Realistic morphological data was investigated by varying the lipid core length ( $1 \leq l \leq 8$ , in mm), the stenosis ratio ( $46.7 \leq sr \leq 66.7$ , in %), the fibrous cap thickness ( $0.025 \leq fc \leq 0.25$ , in mm) and the lipid core width ( $30 \leq w \leq 90$ , in %) [18]. The values of the geometrical parameters used to define the idealized coronary plaque models are shown in Table 2.1.

Level	$l[\text{mm}]$	$sr[\%]$	$fc[\text{mm}]$	$w[\%]$
1	1	46.7	0.025	30
2	2	53.3	0.05	45
3	4	56.7	0.1	60
4	6	60	0.15	75
5	8	66.7	0.25	90

Table 2.1: Geometrical parameters used to generate the parametric 3D models.

Residual stresses (RS) in longitudinal and circumferential directions were incorporated into the model to analyze the influence of the important mechanical factors in the vulnerability of the plaque.

In order to assess the role of circumferential and axial residual stresses on the atheroma plaque ruptures, the set of 625 simulations described in the previous subsection (Subsection 2.1.2) were performed under three different hypothesis;

- (i) without RS,
- (ii) just considering axial RS
- (iii) and taking account both circumferential and axial RS.

In total, 1875 (625 x 3) analyses have been performed.

### 2.1.3 Mesh

A fine mesh was created in the various regions of the model and the fibrous cap region was meshed with an adaptive mesh. Previous sensitivity analyses were performed on the mesh to choose the definitive one. Due to the symmetry of the problem only a quarter of the model with approximately 150.000 linear and hybrid tetrahedral elements and 30.000 nodes was considered. In general, the hybrid elements are used for incompressible materials to avoid volumetric locking.

The mesh used and the number of nodes and elements vary from one simulation to another due to the geometry undergoes small alterations as the parameters are changed. Figure 2.2 show a transversal section of the mesh corresponding to one of the 625 models simulated.

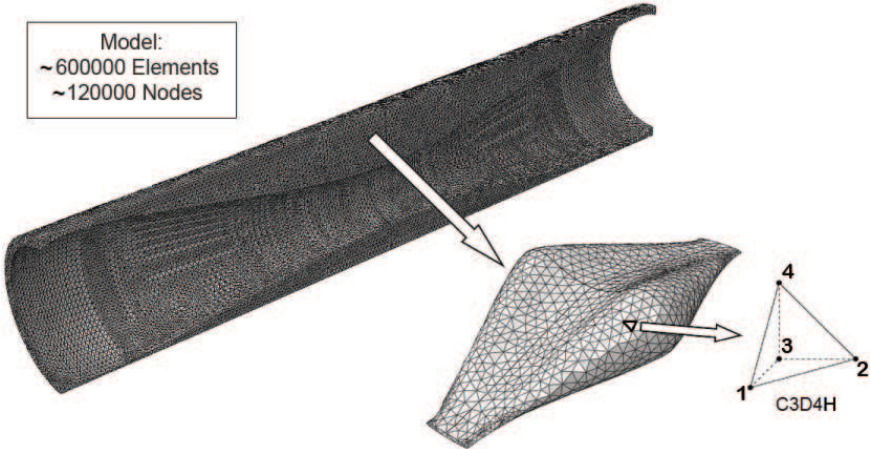


Figure 2.2: Longitudinal section of the mesh used for one of the 625 models simulated. Detail of the lipid core mesh. C3D4 is the kind of elements used which correspond to a linear and hybrid tetrahedral elements.

### 2.1.4 Material properties

All tissues were modelled as nonlinear, hyperelastic and incompressible materials [9, 28]. The lipid core and the atherosclerotic plaque were modelled as isotropic materials, while healthy wall was considered as an anisotropic material with two families of fibres, oriented at  $\pm 61.8^\circ$  and  $\pm 28.35^\circ$  with respect to the circumferential direction in the adventitia and the media layers, respectively. Both families of fibres were assumed to have the same mechanical properties [28] (see Figure 2.3).

The behaviour of the tissue was modelled by using the Gasser, Ogden and Holzapfel (GOH) strain energy function (SEF) [22]

$$\Psi = \mu[I_1 - 3] + \frac{k_1}{2k_2} \sum_{i=4,6} \exp(k_2[\kappa[I_1 - 3] + [1 - 3\kappa][I_i - 1]]^2) - 1, \quad (2.1)$$

where  $\mu > 0$  and  $k_1 > 0$  are stress-like parameters and  $k_2 > 0$  and  $0 \leq \kappa \leq \frac{1}{3}$  are dimensionless parameters (when  $\kappa=0$  the fibres are perfectly aligned (no dispersion) and when  $\kappa=\frac{1}{3}$  the fibres are randomly distributed and the material becomes isotropic),  $I_1$  is the first invariant of  $\mathbf{C} = \mathbf{F}^T \mathbf{F}$  with  $\mathbf{F}$  the deformation gradient tensor,  $I_4 = \mathbf{m}_0 \cdot \mathbf{C} \mathbf{m}_0$  and  $I_6 = \mathbf{n}_0 \cdot \mathbf{C} \mathbf{n}_0$  are invariants which depend on the direction of the family of fibres at a material point  $\mathbf{X}$  that is defined by the unit vectors field  $\mathbf{m}_0$  and  $\mathbf{n}_0$  [58].

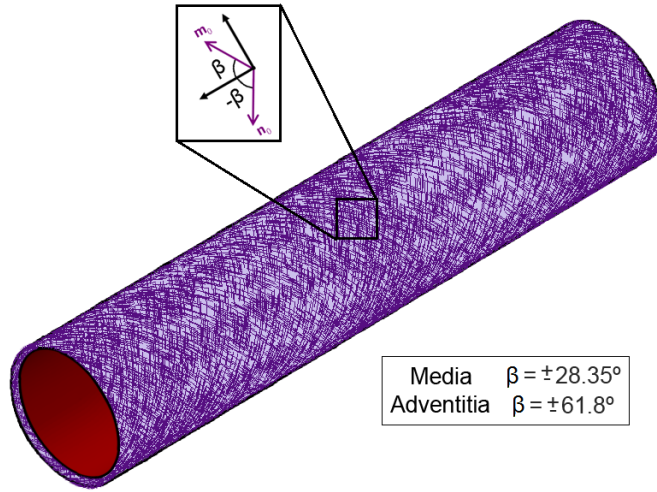


Figure 2.3: Fibres distribution in the adventitia and media layers.  $\pm \beta$  is the orientation angle of the fibres with respect to the circumferential direction.  $\mathbf{m}_0$  and  $\mathbf{n}_0$  are the vectors which define the fibre orientations of each family of fibres.

To obtain the material parameters for the constitutive law of the tissue, experimental data presented in previous works (the adventitia and the media properties from Holzapfel et al. [28] and the plaque and the lipid core properties from Versluis et al. [67]) were fitted using the Levenberg–Marquardt minimization algorithm [43].

Figure 2.4 shown the experimental stress-stretch model responses for each part of the model considered [28, 67]. Adventitia and media layers have different behaviour in the longitudinal and circumferential direction due to its anisotropy.

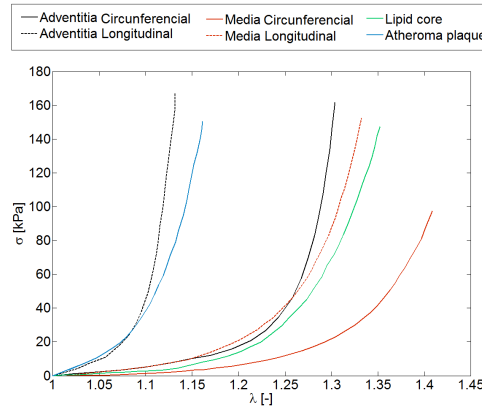


Figure 2.4: Stress-stretch model responses of experimental data taken from the literature for each tissue of the model considered; adventitia and healthy media layers in both directions (circumferential and longitudinal), lipid core and atheroma plaque.

Table 2.2 shows the results of the parameter identification for each tissue fitted according the Gasser, Ogden and Holzapfel strain energy function [22]. Furthermore, the normalized mean square root error ( $\varepsilon$ ) which is defined as

$$\varepsilon = \frac{\sqrt{\frac{\chi^2}{n-q}}}{\mu}, \quad (2.2)$$

was used to check the goodness of the fit. Where  $q$  is the number of parameters of the (SEF),  $n$  is the number of data points,  $n - q$  is the number of degrees of freedom, and  $\mu$  is the mean stress.

	$\mu [kPa]$	$k_1 [kPa]$	$k_2 [-]$	$\kappa [-]$	$\varepsilon [-]$
Adventitia	8.44	547.67	568.01	0.26	0.041
Healthy media	1.4	206.16	58.55	0.29	0.014
Atheroma plaque	9.58	17654.91	0.51	0.33	0.056
Lipid core	0.052	965.76	70	0.33	0.03

Table 2.2: Material parameters used in the finite element analysis for the adventitia, the healthy media, the atheroma plaque and the lipid core.

### 2.1.5 Boundary conditions

Regarding the boundary conditions, the longitudinal displacements were constrained at the end of the vessel, whereas the radial displacement was allowed, to avoid the solid rigid behaviuor of the model. Symmetry conditions were imposed in the corresponding symmetry planes due to only a quarter of the model was simulated.

Firstly, in order to introduce the circumferential residual stress, a cut with an opening angle of  $23.5^\circ$  was performed in the opposite side of plaque location according to the experimental data of severe atherosclerosis obtained by Jaroslav et al. [32]. The opened model was closed such that we finally obtain the configuration shown in Figure 2.5.a. Secondly, to introduce the longitudinal residual stress, the model was stretched a 4.4 % of the vessel length in the longitudinal direction, representing in-vivo conditions [28] as it shown in Figure 2.5.b. Thirdly, a constant internal pressure of 140 mmHg (18.7 kPa) was imposed in the inner surface of the lumen, simulating the blood flow pressure [48] (Figure 2.5.c).

In the set of simulation without RS just the internal pressure is applied (Figure 2.5.c), in the set of simulation with the longitudinal RS included the second and third boundary condition are applied (Figure 2.5.b + Figure 2.5.c), and finally, in the set of simulation with longitudinal and circumferential RS included, the three boundary conditions are applied (Figure 2.5.a + Figure 2.5.b + Figure 2.5.c).

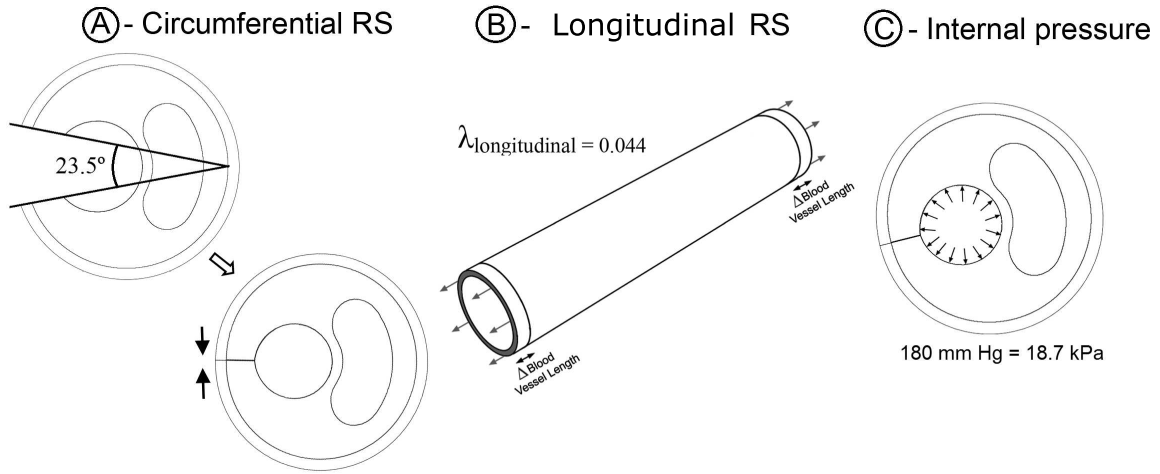


Figure 2.5: Boundary conditions applied for the different simulation set. A - Circumferential RS. B - Longitudinal RS and C - Internal Pressure.

Maximal Principal Stresses (MPS) were considered as the mechanical factor for the purposes of comparison in this study.

## 2.2 Results

It is important to remark that the maximum MPS was measured at the critical zones and always appeared in the circumferential direction. Some authors have shown that the maximum MPS sometimes appears at healthy areas, where rupture is unlikely [60, 61, 59]. Healthy areas where rupture is not probable, even if a local stress maximum occurred there, have been excluded from the analysis of the results.

### 2.2.1 Statistical Analysis

To assess the influence of the geometrical parameters on the MPS, a statistical analysis was performed. The Lilliefors test (checking the normality of the distribution), the Student's t-Tests and the analysis of variance (ANOVA) were used. The ANOVA test and the Student's t-Test were performed at 1% and 5% significance level, respectively. Figure 2.6 shows the statistical analysis performed on the maximum MPS value in the critical region with respect to the distinct geometrical parameters for the three different studied cases, respectively. Each subfigure represents the results grouped for the different levels of each geometrical parameter, and the variation of this parameter becomes influential if the MPS is modified significantly as this parameter varies. In this Figure, the means of group  $n$  and the groups marked with  $*(n)$  are significantly different with the probability ( $p$ ) indicated in the legend which is located in the top of each figure. Subfigures without any mark

mean performing two sample comparisons, the means are always significantly different. On each box, the central mark is the median, the edges of the box are the 25th and 75th percentiles, the whiskers extend to the most extreme data points not considered outliers, and outliers are plotted individually.

In the first row of Figure 2.6, the median for each variation of the lipid core length increases slightly with the lipid core length for all the cases, especially in the axial and circumferential RS case. For the cases with axial RS and without RS, considering all the two-sample comparisons (paired t-test), some significant differences are found, between the second group ( $l = 2$  mm) and the groups marked with  $^{(2)}$  and between the fifth group ( $l = 8$  mm) and the groups marked with  $^{(5)}$  ( $p < 0.01$ , see Figure 2.6). However, when the circumferential and the axial RS are considered, the lipid core length becomes more influential since the means are always significantly different for all the two-sample lipid core length comparisons considered ( $p < 10^{-5}$ ).

The stenosis ratio statistical analysis is shown in the second row of the Figure 2.6. The medians and the dispersion are similar and very few significant differences between the means of the groups for the three cases considered are found, showing that the stenosis ratio do not play a significant role in vulnerability related with the MPS.

The statistical analysis of the fibrous cap thickness is shown in the third row of Figure 2.6 and proves the influence of this parameter on the MPS for the three analyzed simulations set. A noteworthy remark is that the median and the dispersion of each variation of the fibrous cap thickness decreases dramatically as the fibrous cap thickness increases. Considering all the two-sample fibrous cap thickness combinations, the means are always significantly different ( $p < 10^{-5}$ ), reflecting the huge influence of this parameter on the MPS values, even if the RS are not considered.

Finally, the lipid core width statistical analyses shown in the fourth row of Figure 2.6, shows that both medians and dispersions increase with the lipid core width. In a similar way than in the case of the fibrous cap thickness, for all the two-sample lipid core width considered comparisons, the means are always significantly different ( $p < 10^{-5}$ ) for the three studied cases, showing again a high dependence on this parameter.

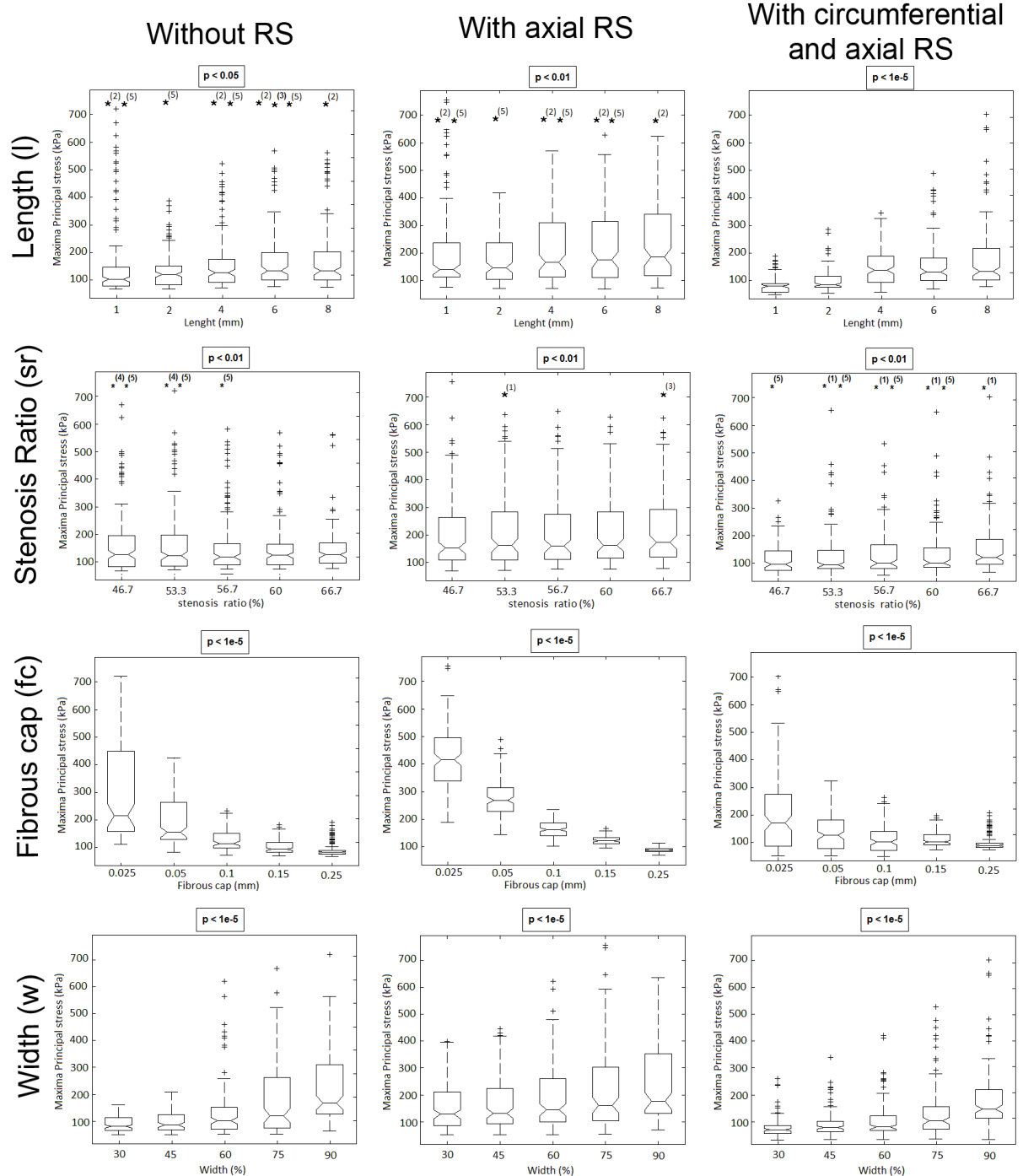


Figure 2.6: Statistical analysis: Maximum MPS vs. the variation of each parameter for the three different cases; without RS, with the axial RS included and with the circumferential and the axial RS included.

### 2.2.2 Trend analysis

In order to compare the variation of circumferential stress versus geometrical parameters, a normalized variation of each parameter has been defined. This parameter ( $\nu$ ) is obtained as  $\nu = \frac{a-a_0}{a_1-a_0}$ , where the variable “ $a$ ” represents each of the four parameters (lipid core length ( $\nu_l$ ), lumen radius ( $\nu_r$ ), fibrous cap thickness ( $\nu_{fc}$ ) and lipid core width ( $\nu_w$ )) in whatever position, and  $a_0$  and  $a_1$  are the lowest and highest values respectively of each parameter. Figure 2.7 represents the maximum MPS vs. normalized variation  $\nu$  of each parameter. There are 5 variations for each parameter, therefore 125 cases have been represented in each normalized variation of each parameter.

A trend analysis has been performed in order to show the influence of the variation of each parameter in the maximum MPS. Therefore, a linear trendline ( $\sigma(kPa) = p_1\nu + p_2$ ) has been added to the experimental data in each graph. The general trend observed is that the maximum MPS increases respect to the cases without RS if axial RS are considered, whereas the MPS decreases and the dispersion is reduced if circumferential and axial RS are included, as Figure 2.7 shown.

In the first subfigure of Figure 2.7 the linear trendline has a positive gradient for the three cases studied ( $p_1 = 37.48kPa$ ,  $p_1 = 45.3kPa$ ,  $p_1 = 98.2kPa$  for the case without RS, with circumferential RS included and axial and circumferential RS included, respectively) and  $p_1$  increases more than twice from the cases without RS to those with axial and circumferential RS included, reflecting an increased influence of this parameter on the MPS when the axial and circumferential RS are considered.

Stenosis ratio evolution (second subfigure of Figure 2.7) has negative gradient for the cases without RS included ( $p_1 = -32.6kPa$ , so maximum MPS decreases as the lumen radius increases from 167.3 kPa to 134.7 kPa for  $sr = 46.7\%$  and  $sr = 66.7\%$ , respectively). However,  $p_1$  is positive for the cases with RS considered, so the general trend changes and maximum MPS increases as the lumen radius increases when RS are taken account. Furthermore, the gradient concerned to the stenosis ratio are the lowest, reflecting again a low influence of this parameter on the MPS.

The gradients related to the fibrous cap thickness (third subfigure of Figure 2.7) are the steepest and they are negative ( $p_1 = -204.7kPa$ ,  $p_1 = -293.6kPa$ ,  $p_1 = -58.8kPa$  for the case without RS, with circumferential RS included and axial and circumferential RS included, respectively).

Finally, the lipid core width analysis, (fourth subfigure of Figure 2.7), shows a pronounced slope with a positive value for the three set of cases studied (with axial RS, with circumferential and axial RS and without them). Eventually,  $p_1$  decreases from the case without RS to the cases with RS considered.

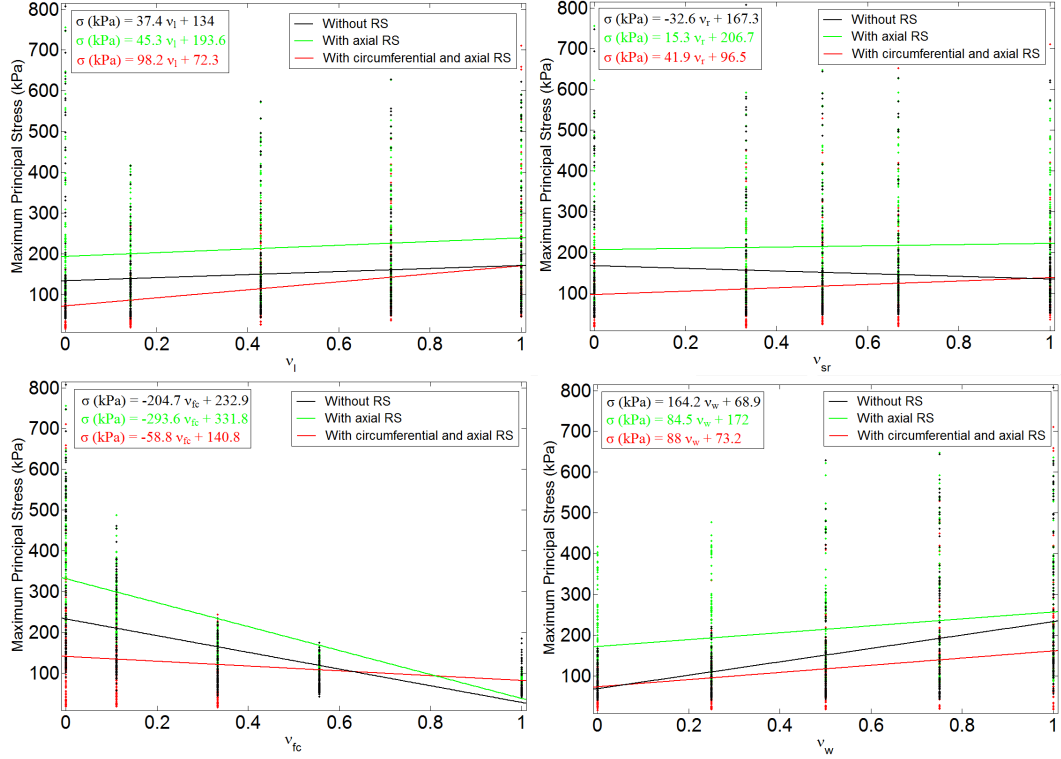


Figure 2.7: Maximum MPS vs. the variation of each normalized parameter. Linear polynomial approximation is included ( $\sigma = p_1v + p_2$ ).

### 2.2.3 Vulnerability study

Regarding the vulnerability of the plaque, different threshold stress values have been proposed by different authors [39, 10, 42, 49]. In this study, a threshold value of 247 kPa has been used according to the set of experimental data obtained by Loree et al. (1994), assuming a normal distribution of the data. This threshold value indicates that the probability of having plaque rupture is 0.95 for the cases whose combination of parameters have a maximum MPS equal or higher than 247 kPa, according to the data by Loree et al. (1994).

The maximum MPS for each combination of parameters is shown in Figure 2.8 and 2.9. In Figure 2.8, the two most influential parameters, the fibrous cap thickness and the lipid core width ( $fc$  and  $w$ ), were chosen as the variable represented by the surfaces. In each subfigure, five surfaces are presented, one for each  $sr$  variation. The safety threshold plane at 247 kPa is presented. The results obtained for the three cases (with axial RS, with circumferential and axial RS and without them) have been compared both in Figure 2.8 and 2.9.

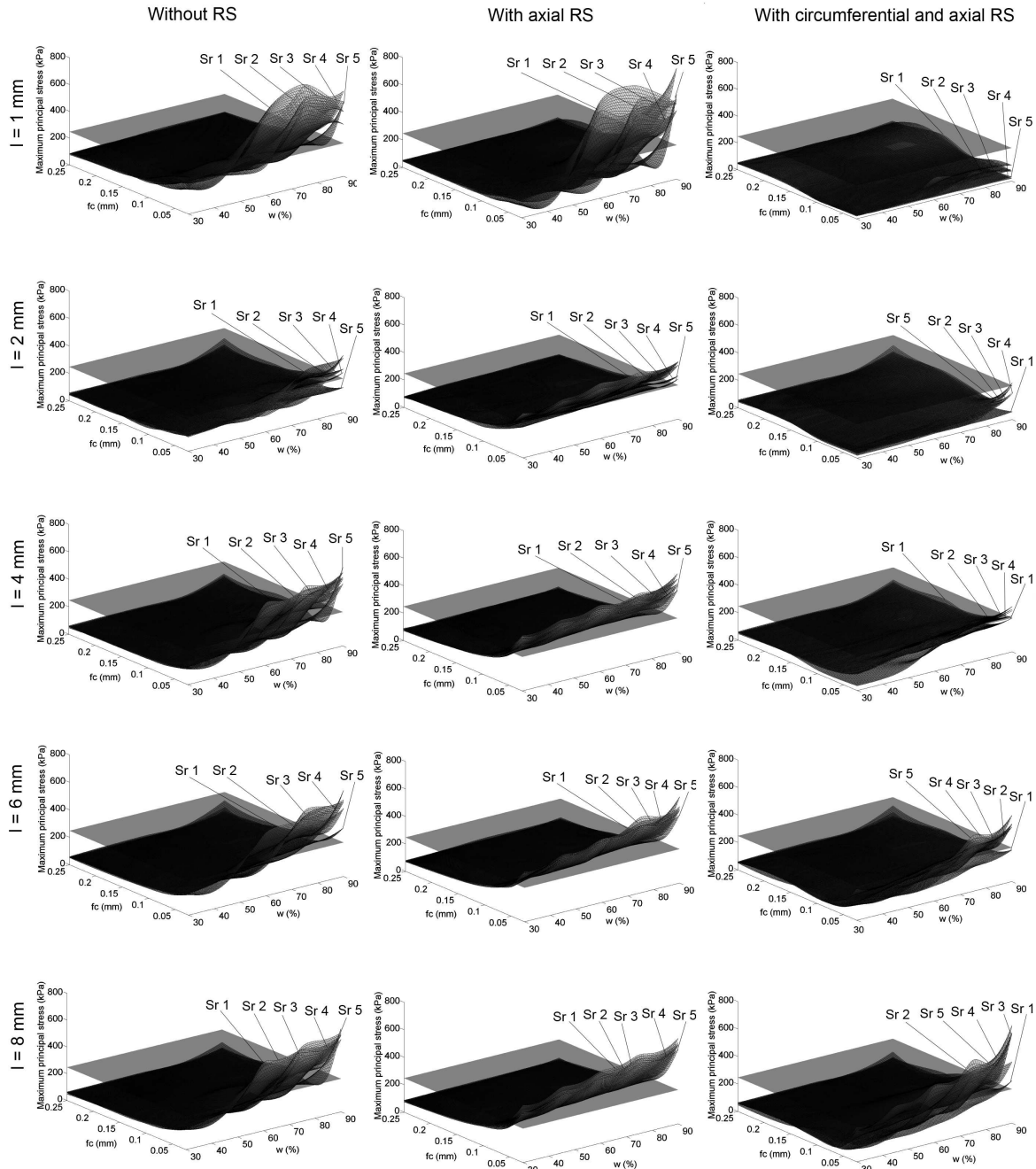


Figure 2.8: Maximum MPS surfaces for a given lipid core length for the three cases studied; Without RS, with the axial RS included and with the circumferential and the axial RS included.

For the sake of clarity, the contour maps of the maximum MPS that are higher than the safety threshold plane (the intersections between each surface of Figure 2.8 and the safety threshold of 247 kPa plane for a lipid core length given) are shown in Figure 2.9. According to the literature, the fibrous cap thickness has been considered to be the most important risk factor for the plaque rupture, but it is not the only one.

Interestingly, the obtained contour maps change for the different studied cases. For the case without RS, similar contour maps are obtained for  $l=4$  mm,  $l=6$  mm and  $l=8$  mm, showing that the MPS has a strong dependency on the lipid core width (vulnerability limit of  $w > 60\%$ ). Despite the fact that the lines corresponding to each variation of  $sr$  intersect in some cases, the vulnerability area increases as the stenosis ratio decreases. In every case, the vulnerable threshold of the fibrous cap thickness is between 0.025 and 0.01 mm.

However, the obtained contour maps can be classified into two groups according to the value of the lipid core length if axial RS are included, showing the high dependency on that parameter of the MPS. The first group includes the small atheroma plaques ( $l \leq 2$  mm), the lipid core width and the stenosis ratio have an important influence on the MPS (atheroma plaque becomes vulnerable for  $w > 50\%$ ). The second group includes the long ones ( $l \geq 4$  mm), the influence of  $w$  is less important, being more vulnerable for high values of  $w$ . A linear trendline is observed, being the vulnerable fibrous cap thickness threshold around 0.05 mm for low  $w$  values and 0.075 mm for high  $w$  values. Again, despite the fact that the lines corresponding to each variation of  $sr$  intersect in some cases, the vulnerability area increases as the stenosis ratio decreases.

Finally, if circumferential and axial RS are included, the obtained contour maps can be also classified into two groups as a function of the lipid core length, showing a strong dependency on that parameter of the MPS. First group for the small atheroma plaques ( $l \leq 2$  mm), where there is not vulnerable geometries, and second group for the long ones ( $l \geq 4$  mm), where the influence of  $w$  is important (atheroma plaque become vulnerable for  $w > 55\%$ ). In every case, the vulnerable fibrous cap thickness threshold is around 0.05 mm.

It can be seen that the axial residual stresses reduce the dependency between the MPS and the lipid core width except for the smallest lipid core length ( $l=1$  mm). Interestingly, the axial residual stresses dramatically increase the vulnerable area showing MPS values higher than 247 kPa for small values of the lipid core width. However, the circumferential and the axial residual stresses together produce again a strong dependency between the MPS and the lipid core width, and the vulnerable area highly decreases due to the effects of compression stress in the inner layer of the vessel fibrous cap zone, produced by the circumferential RS. This fact shows the relevance of considering the residual stresses in the vulnerability computational analysis of the plaque.

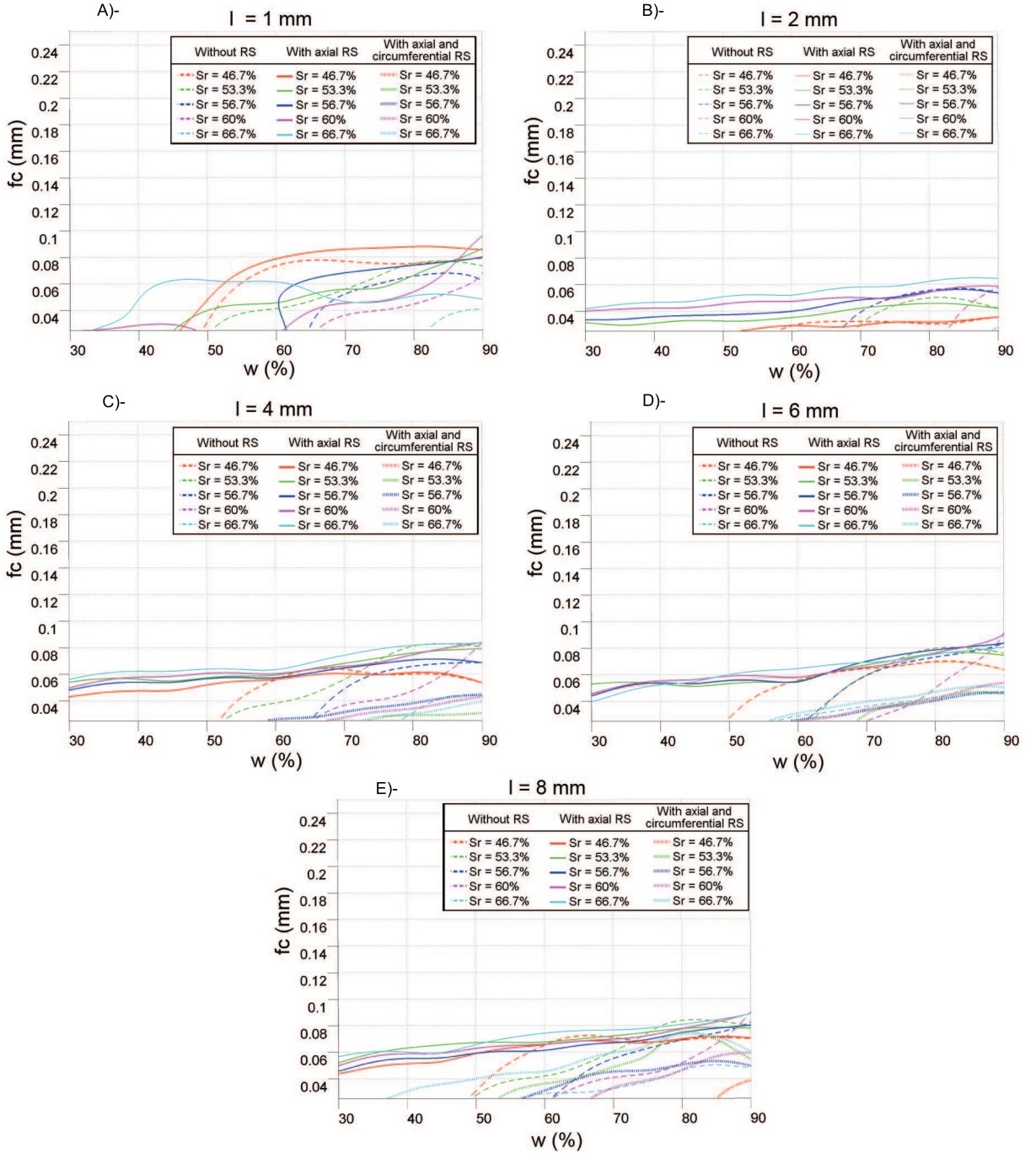


Figure 2.9: Contours of the intersection between the safety threshold plane (247 kPa) and the maximum MPS surfaces for all  $l$  studied and for the results without RS, with the axial RS included and with the circumferential and the axial RS included.

Figure 2.10 illustrates the difference between the results obtained in an idealized 3D model with the longitudinal RS included (Figure 2.10.a), a 3D model with the circumferential and the longitudinal RS included (Figure 2.10.b) and the equivalent 3D model without residual stresses (Figure 2.10.c). The dimensions of the presented case are; 4 mm long lipid core, 53.3% of stenosis ratio, 0.025 mm thick of fibrous cap and 60% of lipid core width. The maximum MPS is located at the fibrous cap in every case, however its value varies from 451.7 kPa in the model with the axial RS included, to 254.4 in the with circumferential and the axial RS included and to 385.7 kPa in the model without residual stress effects. The maximum MPS decreases with the incorporation of circumferential and axial RS, but increases when just the longitudinal RS are considered. However, although this trend is observed in a great number of cases, it could not be completely generalized. It also highly depends on the geometrical factors, as it is shown in Figure 2.9.

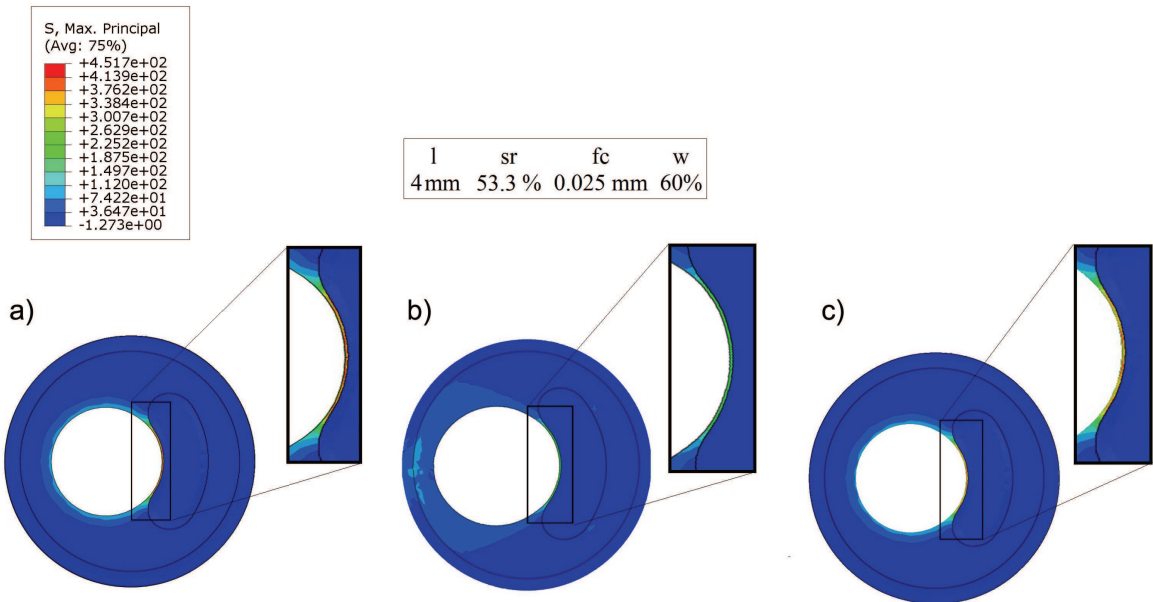


Figure 2.10: Contour maps of MPS. Comparison between a model with the longitudinal RS included (a), a model with the longitudinal and the circumferential RS included (b) and without them (c).

#### 2.2.4 Vulnerability factor

In order to quantify the vulnerability risk, a vulnerability factor (*VF*) was used. This factor is defined as

$$VF = \frac{\text{Maximum MPS (kPa)}}{\text{Critical MPS (kPa)}}, \quad (2.3)$$

where the critical MPS value is assumed to be 247 kPa.

For the 625 cases in which circumferential and axial RS were included, the value of the  $VF$  for the main combinations of parameters which produce a maximum MPS higher than 247 kPa (Figure 2.9) are shown in Table 2.3, 2.4 and 2.5. In each table, the lipid core width is considered constant, the fibrous cap thicknesses are 0.025 mm (left sides of the tables) and 0.05 mm (right sides of the tables) and the lipid core length and the lumen radius vary.

Generally, the  $VF$  values in Tables 2.4 and 2.5 are higher than in Table 2.3 for the same values of  $l$  and  $sr$ , showing the dependency on  $w$  of MPS. It can be observed that the  $VFs$  increase with  $w$ . Most of the  $VFs$  are lower than 1 for the small values of  $l$  ( $l \leq 2$  mm) and higher than 1 for the long ones ( $l \geq 4$  mm), which show the dependence on  $l$  of MPS. A positive relation was observed between the increase of  $fc$  and the  $VF$  since the values of the  $VFs$  are significantly higher in the left sides of the tables ( $fc = 0.025$  mm) than in the right sides ( $fc = 0.05$  mm). The highest vulnerability factor is 2.98 ( $l = 8$  mm,  $sr = 66.6\%$ ,  $fc = 0.025$  mm and  $w = 90\%$ ), exceeding the safety threshold value of 247 kPa by a factor of three, Table 2.5.

sr(%) l(mm)	fc = 0.025 mm					fc = 0.05 mm				
	1	2	4	6	8	1	2	4	6	8
46.6	0.08	0.16	0.73	0.44	0.51	0.09	0.10	0.52	0.41	0.47
56.3	0.66	0.20	0.75	0.52	1.66	0.09	0.20	0.25	0.39	0.41
56.6	0.11	0.27	1.02	1.02	1.12	0.11	0.19	0.72	0.59	0.68
60	0.14	0.19	0.98	1.00	0.79	0.10	0.20	0.68	0.41	0.44
66.6	0.28	0.51	0.80	1.10	1.70	0.23	0.38	0.63	0.75	0.89

Table 2.3: Vulnerability factors for  $fc = 0.025, 0.05$  mm and  $w = 60\%$ .

sr(%) l(mm)	fc = 0.025 mm					fc = 0.05 mm				
	1	2	4	6	8	1	2	4	6	8
46.6	0.08	0.18	0.86	0.71	0.79	0.08	0.11	0.61	0.52	0.63
56.3	0.59	0.44	1.04	1.52	1.82	0.35	0.39	0.67	0.65	1.09
56.6	0.11	0.32	1.16	1.31	2.14	0.10	0.25	0.81	0.72	0.85
60	0.55	0.22	1.10	1.64	1.70	0.11	0.23	0.77	0.52	0.59
66.6	0.32	0.59	1.05	1.34	1.94	0.25	0.47	0.71	0.88	1.16

Table 2.4: Vulnerability factors for  $fc = 0.025, 0.05$  mm and  $w = 75\%$ .

sr(%) / l(mm)	fc = 0.025 mm					fc = 0.05 mm				
	1	2	4	6	8	1	2	4	6	8
46.6	0.08	0.23	1.00	0.93	1.25	0.08	0.14	0.67	0.71	0.85
56.3	0.48	0.79	1.05	1.69	2.67	0.45	0.36	0.82	0.89	1.12
56.6	0.13	0.76	1.33	1.70	1.80	0.10	0.30	0.93	0.91	0.98
60	0.30	1.02	1.25	1.95	2.64	0.36	0.45	0.92	1.07	1.19
66.6	0.33	1.08	1.21	1.61	2.98	0.27	0.47	0.86	1.00	1.25

Table 2.5: Vulnerability factors for  $fc = 0.025, 0.05$  mm and  $w = 90\%$ .

## 2.3 Importance of 3D models

Up to now, parametric studies have been performed in two dimensions(2D) assuming the plane strain hypothesis [10, 37, 17, 49, 48] in order to define the site of MPS concentrations. Nevertheless, other studies show that a 2D structural analysis tends to overestimate the amplitude of the PCS [49]. 3D finite element models of atherosclerotic coronaries may be very valuable and more accurate than the 2D finite element analysis in helping cardiologists evaluate the risk of spontaneous plaque rupture in a patient. Therefore, the aim of this section is to compare the results obtained by a 3D model with the plane strain model usually employed in the literature to study the vulnerability of plaque [50, 6, 49, 67, 47, 48].

Since both models should be simulated with the same dimensions, boundary conditions and material properties, a 3D model without axial and circumferential RS included has been chosen to compare with the equivalent plane strain model. Longitudinal RS does not make sense in the plane strain model, and 3D models with just circumferential RS implemented have not been considered.

The plane strain model have been obtained from the central cross section of the equivalent 3D model. This section was extruded at a small length in order to introduce some purely 3D parameters such as the fiber orientation.

The MPS distribution of the central cross section of both models are shown in Figure 2.11. The dimension of the presented case are; 2 mm long lipid core, 46.6 % of stenosis ratio, 0.025 mm thick of fibrous cap and 90 % of lipid core width. The maximum MPS is located in the fibrous cap in both cases, however it is about 205 kPa in the 3D model vessel (2.11.a) and 510 kPa (2.11.b) in the plane strain vessel. According to the threshold value of 247 kPa proposed by Lendon et al. [39], Cheng et al. [10], Loree et al. [42], Ohayon et al. [49], the 3D plaque model could be considered stable (maximum MPS is lower than 247 Kpa), but the plane strain plaque model could be considered vulnerable (maximum MPS is much greater than the threshold value).

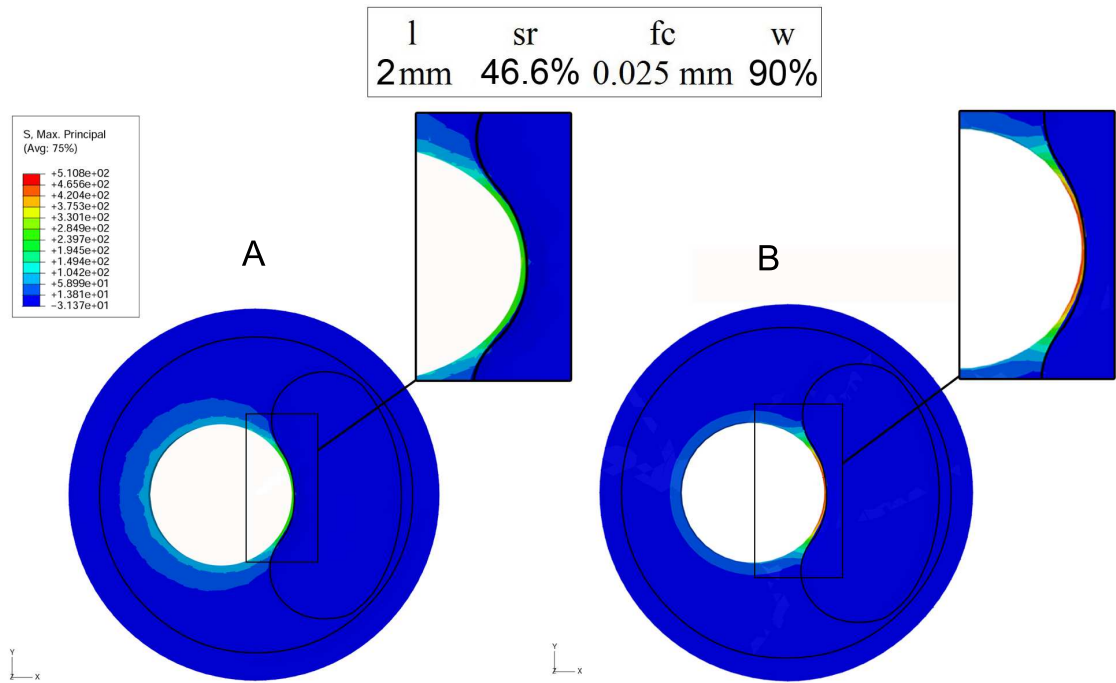


Figure 2.11: MPS (kPa). Comparison between 3D and plane strain plaque model. A - 3D model vessel. B - Plane strain model.

# Chapter 3

## REAL GEOMETRY VERSUS IDEALIZED GEOMETRY

In order to validate the assumption of an idealized geometry of the atherosclerotic artery, a patient-specific geometry of a coronary vessel has been segmented and modelled using the same material parameters, boundary conditions and dimensions. The performance of the 3D model used to carried out the 3D parametric analysis have been compared with a *in-vivo* reconstruction .

A real geometry of a left coronary artery with atherosclerosis disease was obtained by *in-vivo* intravascular ultrasound (IVUS) images. The artery, which belong to an adult male patient of 50 years old, was imaged using an automatic pullback with a speed of 0.5mm/s, from the distality of the lesion to the tip of the guiding catheter, Figure 3.1.a. The MIMICS 10.0 commercial code was used to reconstruct the 20 cross-sections of the human coronary vulnerable plaque. The 3D plaque geometry of the patient is reconstructed by piling up and following the trajectory of the center of the catheter, Figure 3.1. Plaque components were characterized by their appearance on IVUS images, the contours delimiting lumen border, media, adventitia and plaque components (lipid core and atheroma plaque) were manually traced on each IVUS cross-sectional image.

Figures 3.1.b and Figure 3.1.c show a cross and transversal section, respectively, of the 3D *in-vivo* atherosclerotic vessel obtained by IVUS. A noteworthy remark is that the cross section obtained by IVUS shown in Figure 3.1.a is the same cross section as that shown in 3.1.b.

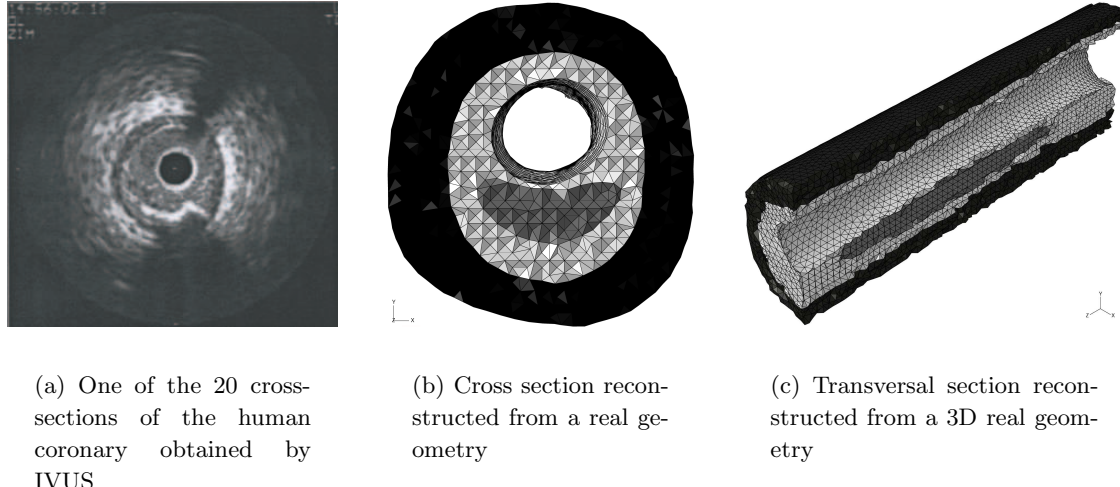


Figure 3.1: 3D reconstruction of a vessel with atherosclerotic lesion obtained by IVUS. Notice that the cross section obtained by IVUS (a) is the same cross section as that shown in (b).

Dimensions of lipid core and fibrous cap thickness were measured in the geometrical reconstruction from the IVUS for the purposes of comparison with a case with similar dimensions and properties in the 3D parametric study. The model was meshed with 252.216 linear tetrahedral elements of type C3D4H of similar size to those of the 3D parametric mesh, and 52.312 nodes, Figures 3.1.b and 3.1.c.

The dimensions measured on the real geometry obtained by IVUS images are shown in Table 3.1.

$l(\text{mm})$	$r(\text{mm})$	$fc(\text{mm})$	$w(\%)$
10	0.7	0.04	55

Table 3.1: Parameters measured in the 3D reconstruction of a vessel with atherosclerotic lesion obtained by IVUS

Amongst all the 3D parametric models, the geometry with more similar parameters to the real geometry segmented from IVUS has been chosen, see Table 3.2. The lipid core length is 2 mm shorter in the idealized geometry than in the specific-patient model because 8 mm is the largest value studied for the lipid core length in the parametric study. However, Figure 2.9.a shows that the influence of lipid core length variation on the maximum MPS is not relevant for long lipid core lengths, so this can be considered as a good approximation. Furthermore, in order to simplify the finite element analysis, both models (idealized and patient-specific) have been simulated without RS.

$l$ (mm)	$r$ (mm)	$fc$ (mm)	$w$ (%)
8	0.7	0.05	60

Table 3.2: Parameters selected to compare the idealized 3D with the real geometry. Note that the lipid core length is 2 mm shorter, however Figure 2.9.a shows that the influence of lipid core length variation is not relevant for long lipid core lengths.

Both in the real reconstructed vessel and in the idealized model, the spatial distribution of the MPS is quite similar and the maxima are both located in the fibrous cap. The maximum MPS of the real and idealized geometries are 322 [kPa] (Figure 3.2.a) and 305 [kPa] (Figure 3.2.b), respectively, showing an error of 5%, and the MPS maps are similar in both cases, showing the validity of the idealized geometry, Figure 3.2. In both models the maximum MPS is greater than 247 kPa, so according to the defined threshold of 247 kPa defined in previous chapters, both cases could be considered as vulnerable plaque.

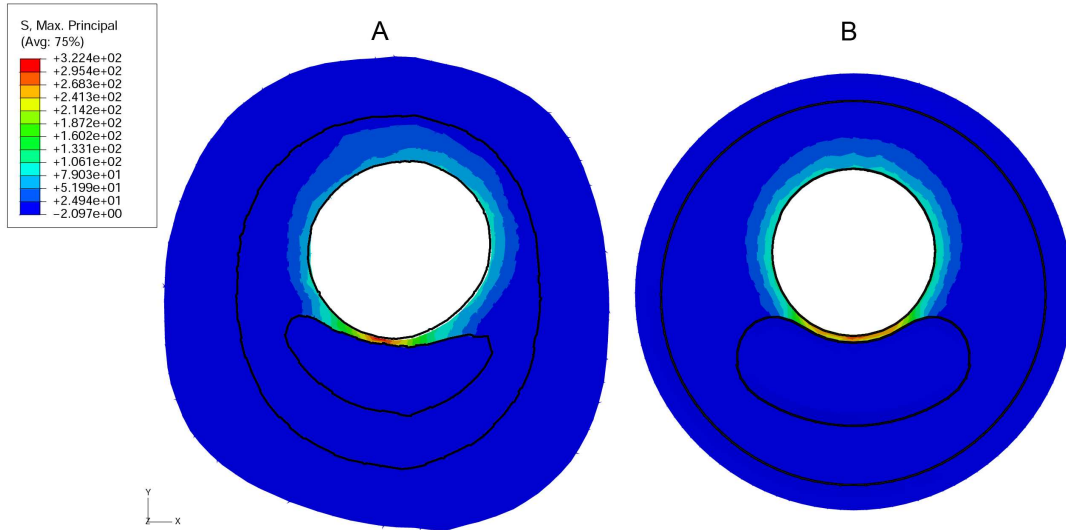


Figure 3.2: MPS distribution (kPa). Comparison between the real geometry reconstructed from the IVUS and the idealized geometry of the 3D parametric study. A - Real geometry reconstructed from the IVUS. B - Idealized geometry.

# Chapter 4

## CONCLUSIONS AND FUTURE WORK

### 4.1 Conclusions

Quantifying the mechanical stress in the wall of an atherosclerotic vessel and, more specifically, in the fibrous cap, is a vital step in predicting the risk of plaque rupture based on biomechanical features, especially in 3D geometries [12]. For this reason, the mechanical behaviour of a 3D parametric atheroma plaque in a coronary vessel with atherosclerosis disease has been studied in this work by varying the four most influential geometrical parameters; lipid core length ( $l$ ), stenosis ratio ( $sr$ ), fibrous cap thickness ( $fc$ ) and lipid core width ( $w$ ), and including RS effects. Static finite element analyses were performed in order to study a group of idealized plaque morphologies and to try to predict the vulnerable plaque rupture.

Furthermore, the performance of 2D plane strain plaque models versus 3D models have been analyzed, concluding that plane strain plaque models are not accurate enough to calculate MPS distribution. Plane strain hypothesis overestimates the maximum MPS, 510 kPa for plane strain versus 205 kPa for 3D analysis in the case presented in Figure 2.11, leading to similar results as those presented by Ohayon et al. [49, 47]. In the case presented here the plane strain analysis exceeds the threshold of 247 kPa, but the 3D analysis does not. This shows the limitation of the plane strain approach for such complex plaques. In addition, Figure 3.2 summarizes a first validation of the 3D idealized model, showing that the 3D model behaves in a very realistic way.

Historically, fibrous cap thickness has been considered the most important and almost the exclusive factor determining plaque vulnerability [4, 8]. To date, very few 3D computational studies have been performed specifically to investigate the effect of the lipid core size on plaque stress distribution. Loree et al. (1992) and Tang et al. (2004) used a finite element model to study the influence of the lipid core width on plaque stress distribution in

a small number of distinct models ( $n=6$  and  $n=3$ , respectively). Imoto et al. (2005) came to the conclusion that the size of the lipid core had no influence on the peak circumferential stress, but as their models are particularized to concentric plaques, their conclusions are not generalizable to eccentric coronary lesions. Finet et al. (2004) performed a 2D parametric study which showed that a combination of measures including the arterial remodelling index, the cap thickness, and the necrotic core area or thickness are necessary for prediction. Ohayon et al. (2005) compared the *in-vivo* performance of 2D and 3D finite element models and concluded that 2D analysis tends to overestimate the amplitude of the maximum MPS, however residual stresses are not considered. The distribution of RS and its effects on the stress field in 3D parametric atherosclerotic coronary plaques have never been studied in detail. Owing to the difficulty of estimation stresses and strains in real geometries, the influence of residual stresses is usually ignored in structural analyses intended to predict plaque rupture location. Ohayon et al. [47] assessed RS and its impact on the *in vivo* stress distribution in human vulnerable coronary plaques, studying six real pathological epicardial coronary artery samples.

Regarding the importance of RS, many authors have studied the role of circumferential RS, but mainly in non-stenotic arteries. Holzapfel et al. [28] performed statistical analysis to test for significant correlations between age and axial *in situ* stretch and there were significant negative correlations between both. This suggests that axial *in situ* stretches of the human LAD coronary artery decrease with age. Varnava et al. [65] simulated the effects of tissue aging on residual strain in the main right and left (ramus circumflexus) human coronary arteries, based on experimental data and they found that experimental opening angle scatters considerably with age. The factors affecting the opening angle are age, sex and the degree of atherosclerosis. Besides, their study showed the effect of including the circumferential RS in the final stress distribution. The vessel artery wall is under tension in the inner layers and under compressive stress in the outer layers, for positive opening angles. The difference between both layers increases as the opening angle increases. This fact tends to make the circumferential stress more uniform in the arterial wall under the constant internal pressure.

The findings in the present work show a high dependency on some purely 3D parameters and factors on the MPS distribution, such as the lipid core length and the axial RS, affecting the vulnerability risk of the plaques. Figure 2.9 and 2.10 clearly show the influence of residual stresses since the vulnerable unsafe areas changes when residual stresses are considered. The predominant trend is that the incorporation of axial RS increases the maximum MPS. However, the incorporation of axial and circumferential RS reduces the maximum MPS. Therefore, 3D plaque models could produce more accurate predictions, and plane strain plaque models could not be enough to calculate a sufficiently accurate MPS distribution. Plane strain models not only overestimate the maximum MPS, as it is shown in the literature by Ohayon et al. [49, 35, 47], but they also miss RS effects and

other features as fibre orientation, which can not be consider in 2D models [28].

The general trend observed in this study is that the maximum MPS increases with the lipid core length, the lumen radius and the lipid core width, and also when the fibrous cap thickness decreases. Figure 2.8 and 2.9 and Table 2.3, 2.4 and 2.5 show that the most of the parameter combinations have MPS values lower than 247 kPa ( $VF < 1$ ), however, an important vulnerable plaque region, where the maximum MPS value is higher than the safety threshold ( $VF \geq 1$ ) was found. This region is generally formed by low fibrous cap thickness values. Moreover, this unsafe region changes from the analysis in which axial RS are considered to the analysis in which RS effects are neglected (Figure 2.9) since when just axial RS are included (without internal pressure), the circumferential stresses are positive. Thus, if axial RS and internal pressure is imposed, the circumferential stresses are higher than without considering axial RS. To summarize, the vulnerable plaque region corresponds to a combination of the following parameters:  $w \geq 50\%$ ,  $fc \leq 0.088$  mm for any lumen radius and lipid core length. Table 4.1 shows the  $fc$  and  $w$  vulnerable limits for each  $l$  and for all values of the lumen.

	With axial RS		With circumferential and axial RS		Without RS	
	fc (mm)	w (%)	fc (mm)	w (%)	fc (mm)	w (%)
$l=1$	$fc \leq 0.088$	$w \geq 50\%$	No vulnerable zone		$fc \leq 0.077$	$w \geq 50\%$
$l=2$	$fc \leq 0.085$	No limit	$fc \leq 0.025$	$w \geq 95\%$	$fc \leq 0.050$	$w \geq 58\%$
$l=4$	$fc \leq 0.080$	No limit	$fc \leq 0.052$	$w \geq 62\%$	$fc \leq 0.079$	$w \geq 52\%$
$l=6$	$fc \leq 0.081$	No limit	$fc \leq 0.055$	$w \geq 64\%$	$fc \leq 0.079$	$w \geq 50\%$
$l=8$	$fc \leq 0.082$	No limit	$fc \leq 0.080$	$w \geq 38\%$	$fc \leq 0.080$	$w \geq 50\%$

Table 4.1: Summary of vulnerable limits of  $fc$  and  $w$  for each different  $l$  independently of the  $sr$  parameter.

The fibrous cap thickness and the lipid core width and length have been shown in this study to be critical geometric parameters to the overall plaque stability, whereas it has been shown that the lumen radius influence is lower, but non-negligible. The influence of these parameters on plaque rupture is shown in Figure 2.6.

Similar results were previously obtained by other authors. Ohayon et al. (2008) obtained slight higher limits of these parameters, probably because they performed a 2D study. However, the global trends were similar. The remodelling index (a parameter equivalent to the stenosis ratio) and the lipid core width had a positive correlation with the maximum MPS, while the fibrous cap thickness had a negative correlation with the maximum MPS. Similar trends were found by Virmani et al. (2000) where they suggested that atherosclerotic lesions with a fibrous cap thickness of less than  $65 \mu$  are most likely to rupture. Several studies in the literature shown that plaques containing a highly thrombogenic lipid-rich core are more at risk for rupture if the size of the lipid core is large and is less consistent. Several investigators have reported on the relation of the amount of extracellular gruel and plaque fissuring [23, 14, 51, 15]. Davies et al. [14] estimated that

when at least 40% of the plaque consists of lipid, an atheroma is at risk for rupture.

The 3D parametric study presented on this work can be considered as an additional step towards the development of a tool to assist clinicians in the identification of vulnerable atheroma plaques. The large-scale computational analysis aids the clinical staff to identify the critical morphological parameters that indicate plaque vulnerability and the likelihood of rupture.

## 4.2 Limitations

Some limitations of this study should be mentioned. First, an idealized straight geometry has been used to perform the parametric analysis. Second, the material model was assumed to be isotropic and incompressible for the fibrous plaque and the lipid core and anisotropic and incompressible for the wall vessel. However, these assumptions have been widely accepted as allowable for the assessment of the biomechanical properties of atherosclerotic lesions [10, 41]. Third, the material properties and residual stresses have been taken from experimental data in the literature [32, 28, 67]. There is no data of axial RS for isolated plaques in the literature, so the axial RS used corresponds to a non-stenotic artery. The opening angle was assumed to be constant for all of the geometries though it is known that it depends on the plaque geometry. Fourth, viscoelastic effects were not considered [2, 3, 52]. Fifth, the analysis does not reproduce the pulsatile nature of physiological blood pressure. Also, the fluid-structure interaction effects resulting from such cyclic loading were not considered [34]. It was assumed that there were no shear stresses, torques, time-varying forces or flow-related forces. Only static blood pressure was considered to be acting on the lesion in the models. Nevertheless, it has been documented that the effect of fluid shear stress is insignificant when compared to the effect of tensile wall stresses as a direct component in plaque fracture dynamics [30, 26], although it is considered essential in plaque formation and growth. The estimation of stresses induced by the static pressure load has been proved to be valid to identify stress concentrations in atherosclerotic lesions [10] since the location of stress concentration does not significantly differ between models including static pressure and models with complex dynamic pressure profiles. Sixth, although similar studies in the literature include other parameters such as the lipid core angle or the remodelling index which is related to the lumen radius, the present study takes into account four of the most influential parameters [67, 48]. Several preliminary tests were performed to exclude the lipid core angle as an influential parameter, see Supplementary data. Seventh, calcifications were not considered in order to simplify the study [7]. Different properties of the atheroma plaque were not taken into account in this parametric study. Properties of calcified, cellular and hypocellular plaques have been identified by other authors [42]. Finally, the 3D parametric study only could be validated qualitatively. It is not possible to measure the stress concentration in real

atheroma plaques and to correlate with the main geometrical risk factors *in vivo* conditions and later verify the plaque rupture. Actually, in the literature, the only way to extract stress information is by performing computational simulations reproducing geometry and *in vivo* conditions, and validate the model qualitatively, measuring the geometrical risk factors, but not measuring directly the stresses.

### 4.3 Future work

Following the investigations described in this master work, a number of projects could be taken up, mainly focused on improving the model and its goal of helping to the clinicians to make decisions on atheroma plaque vulnerability.

More careful examination of stress distributions in plaques reveals that it may be caused by the local stress behaviors caused by cap thinning, inflammation, macroscopic heterogeneity, and recently, the presence of microcalcifications, at critical sites. However, the role of microcalcifications is not yet fully understood and most finite element models of blood vessels with atheroma plaque do not take into account the heterogeneity of the plaque constituents at the micro-scale. Some studies indicate beneficial effects in stabilizing the plaque [10, 30], whereas others suggest that the microcalcifications increase the plaque vulnerability and shift the maximal principal stress (MPS) to the region of the microcalcification [7, 71]. Further parametric studies could include microcalcifications and also take into consideration the position and size of the microcalcification as influential parameters on the MPS.

Figure 4.1 shows the central cross section of a possible further parametric study including microcalcifications and considering the microcalcification position angle ( $\alpha$ ), the microcalcification diameter ( $d$ ), the microcalcification eccentricity measured by  $d$  and again the fibrous cap thickness ( $fc$ ) since it is the most influential parameter on the atheroma vulnerability.

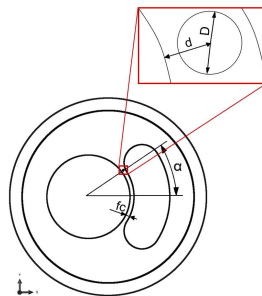


Figure 4.1: Further parametric study. Possible new geometrical parameters related to the microcalcification shown on the cross-section coronary model.

In addition, a 3D model with a eccentric atheroma plaque and negative remodelling have been used in this work, however, other configurations could be analyzed, varying the atheroma plaque distribution (concentric or eccentric) or taking account the remodelling defined by Glagov et al. [24]. Their study demonstrated that coronary arteries can enlarge in response to the development of atherosclerotic plaques. Coronary arteries may respond to plaque growth by either outward expansion of the vessel wall (positive) or vessel shrinkage (negative). The compensatory remodelling process can maintain luminal dimensions during early atherosclerosis. These plaques grow further and the plaque does not generally begin to encroach on the lumen until it occupies 40% of the cross-sectional area. Figure 4.2 summarize other possible configurations of the atheroma plaque.

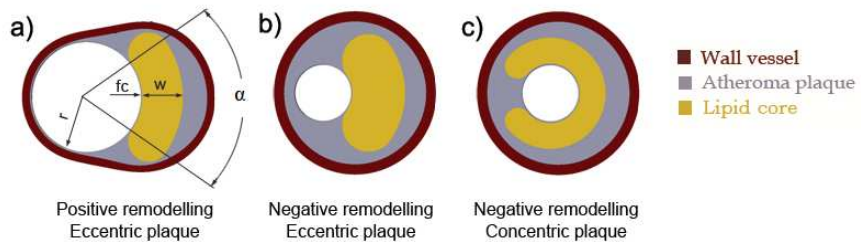


Figure 4.2: (a) Positive arterial growth. (b) Negative arterial growth with an eccentric atheroma plaque. (c) Negative arterial growth with a concentric atheroma plaque.

Finally, it would be of interest to develop a quantitative method for cumulative risk assessment of vulnerable patients based on atheroma plaque morphology which could replace the time consuming biomechanical simulations used in cardiovascular mechanics. A parametric tool based on machine learning techniques (such as Artificial Neural Networks (ANNs) and Support Vector Machines (SVMs) and used to predict the atheroma plaque rupture could be implemented from the results of this 3D parametric study (input). Procedures to detect plaque prone to rupture and to predict rupture location are very valuable for clinical diagnosis. Nowadays clinical procedures for detection of these vulnerable plaques are only performed by image analysis. The use of FEM computations presents the disadvantage of very high computational cost, usually hours or even days, when an immediate response is required. However, FEM analysis are used in pre-operative surgical planning when clinical staff have enough time to perform the computational model and analyze the results. The main objective of this tool would be to search for alternatives to direct FEM simulations in a specific clinical field, detection of vulnerable plaques, when an instantaneous response is needed. Summing up, the procedure proposed would be carried as follows: for a specific patient, clinical staff should measure just four parameters in standard IVUS images and then, by using the ANN or SVM techniques, they would have an immediate response on the atheroma plaque vulnerability. The ANN or SVM

algorithms and the data base would be fed with the results of this study. Figure 4.3 shows an ANN structure proposed to develop the parametric tool described below.

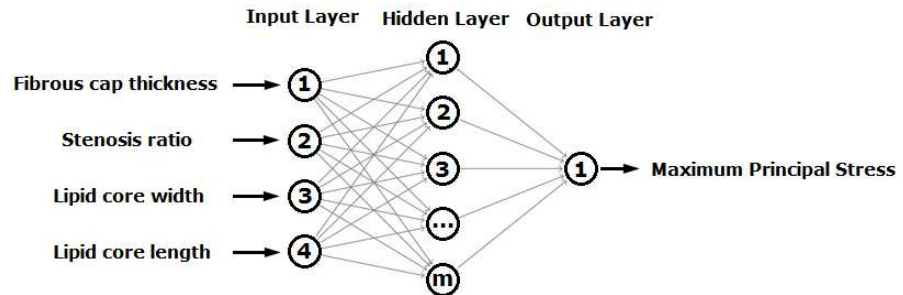


Figure 4.3: Artificial Neural Network structure proposed

# Bibliography

- [1] Allender, S., Scarborough, P., Peto, V., Rayner, M., 2008. European cardiovascular disease statistics 2008 edition. *Health Economics* .
- [2] Armentano, R., Megnien, J. L., Simon, A., Bellenfant, F., Barra, J., Levenson, J., 1995. Effects of hypertension on viscoelasticity of carotid and femoral arteries in humans. *Hypertension* 26, 48–54.
- [3] Armentano, R., Santana, D., Cabrera, E., Graf, S., Perez, H., German, Y. Z., Saldias, M. D. C., Alvarez, I., 2006. An in vitro study of cryopreserved and fresh human arteries: A comparison with eptfe prostheses and human arteries studied non-invasively in vivo. *Cryobiology* 52, 17–26.
- [4] Arroyo, L. H., Lee, R. T., 1999. Mechanisms of plaque rupture: mechanical and biologic interactions. *Cardiovascular Research* 41, 369–375.
- [5] Auer, M., Stollberger, R., Regitnig, P., Ebner, F., Holzapfel, G., 2006. 3-D recon-

struction of tissue components for atherosclerotic human arteries using ex vivo high-resolution MRI. *Medical Imaging* 25, 345–357.

[6] Baldewsing, R. A., de Korte, C. L., Schaar, J. A., Mastik, F., van der Steen, A. F. W., 2004. Finite element modeling and intravascular ultrasound elastography of vulnerable plaques: parameter variation. *Ultrasonics* 42, 723–729.

[7] Bluestein, D., Alemu, Y., Avrahami, I., Gharib, M., Dumont, K., Ricotta, J. J., Einav, S., 2008. Influence of microcalcifications on vulnerable plaque mechanics using FSI modelling. *Journal of Biomechanics* 41, 1111 – 1118.

[8] Briley-Saebo, K. C., Mulder, W. J., Mani, V., Hyafil, F., Amirbekian, V., Aguinaldo, J. G. S., Fisher, E. A., Fayad, Z. A., 2007. Magnetic resonance imaging of vulnerable atherosclerotic plaques: Current imaging strategies and molecular imaging probes. *Journal of Magnetic Resonance Imaging* 26, 460–479.

[9] Carew, T. E., Vaishnav, R. N., Patel, D. J., 1968. Compressibility of the arterial wall. *Circulation Research* 23, 61–86.

[10] Cheng, G., Loree, H., Kamm, R., Fishbein, M., Lee, R., 1993. Distribution of circumferential stress in ruptured and stable atherosclerotic lesions. A structural analysis with histopathological correlation. *Circulation* 87, 1179–1187.

[11] Chun, Y., Dalin, T., Satya, A., 2010. Three-dimensional carotid plaque progression simulation using meshless generalized finite difference method based on multi-year mri patient-tracking data. *Computer Modeling in Engineering & Sciences* 57, 51–76.

[12] Creane, A., Maher, E., Sultan, S., Hynes, N., Kelly, D. J., Lally, C., 2010. Finite element modelling of diseased carotid bifurcations generated from in vivo computerised tomographic angiography. *Computers in Biology and Medicine* 40, 419–429.

[13] Davies, M. J., 1996. Stability and instability: Two faces of coronary atherosclerosis: The Paul Dudley White lecture 1995. *Circulation* 94, 2013–2020.

[14] Davies, M. J., Richardson, P. D., Woolf, N., Katz, D. R., Mann, J., 1993. Risk of thrombosis in human atherosclerotic plaques: role of extracellular lipid, macrophage, and smooth muscle cell content. *British Heart Journal* 69, 377–381.

[15] Douglas, A. F., Christopher, S., Amankulor, N., Din, R., Poullis, M., Amin-Hanjani, S., Ghogawala, Z., 2011. Extracranial carotid plaque length and parent vessel diameter significantly affect baseline ipsilateral intracranial blood flow. *Neurosurgery* 69, 114–121.

[16] Fayad, Z. A., Fuster, V., 2001. Clinical imaging of the high-risk or vulnerable atherosclerotic plaque. *Circulation Research* 89, 305–316.

[17] Finet, G., Ohayon, J., Rioufol, G., 2004. Biomechanical interaction between cap thickness, lipid core composition and blood pressure in vulnerable coronary plaque: Impact on stability or instability. *Coronary Artery Disease* 15, 13–20.

[18] Fujii, K., Carlier, S. G., Mintz, G. S., Wijns, W., Colombo, A., Böse, D., Erbel, R., de Ribamar Costa, J., Jr, Kimura, M., Sano, K., Costa, R. A., Lui, J., Stone, G. W., Moses, J. W., Leon, M. B., 2005. Association of plaque characterization

by intravascular ultrasound virtual histology and arterial remodeling. *The American Journal of Cardiology* 96, 1476 – 1483.

[19] Fung, Y. C., 1993. Biomechanics. Mechanical properties of living tissues. Springer-Verlag.

[20] Fuster, V., Fayad, Z. A., Moreno, P. R., Poon, M., Corti, R., Badimon, J. J., 2005. Atherothrombosis and high-risk plaque: Part II: Approaches by noninvasive computed tomographic/magnetic resonance imaging. *Journal of the American College of Cardiology* 46, 1209–1218.

[21] Gao, H., Long, Q., 2008. Effects of varied lipid core volume and fibrous cap thickness on stress distribution in carotid arterial plaques. *Journal of Biomechanics* 41, 3053 – 3059.

[22] Gasser, T. C., Ogden, R. W., Holzapfel, G. A., 2006. Hyperelastic modelling of arterial layers with distributed collagen fibre orientations. *Journal of The Royal Society Interface* 3, 15–35.

[23] Gertz, S., Roberts, W. C., 1990. Hemodynamic shear force in rupture of coronary arterial atherosclerotic plaques. *The American Journal of Cardiology* 66, 1368 – 1372.

[24] Glagov, S., Weisenberg, E., Zarins, C. K., Stankunavicius, R., Kolettis, G. J., 1987. Compensatory enlargement of human atherosclerotic coronary arteries. *New England Journal of Medicine* 316, 1371–1375.

[25] Hanke, H. Lenz, C. F. G., 2001. The discovery of the pathophysiological aspects of atherosclerosis - A review. *Acta Chirurgica Belgica* 101, 162–169.

[26] Himborg, H. A., Grzybowski, D. M., Hazel, A. L., LaMack, J. A., Li, X.-M., Friedman, M. H., 2004. Spatial comparison between wall shear stress measures and porcine arterial endothelial permeability. *American Journal of Physiology - Heart* 286, H1916–H1922.

[27] Holzapfel, G. A., 2000. *Nonlinear Solid Mechanics*. Wiley, New York.

[28] Holzapfel, G. A., Gasser, C. T., Sommer, G., Regitnig, P., 2005. Determination of the layer-specific mechanical properties of human coronary arteries with non-atherosclerotic intimal thickening, and related constitutive modelling. *American Journal of Physiology-Heart* 289, H2048–H2058.

[29] Holzapfel, G. A., Gasser, T. C., Ogden, R. W., 2000. A new constitutive framework for arterial wall mechanics and a comparative study of material models. *Journal of Elasticity* 61, 1–48.

[30] Huang, H., Virmani, R., Younis, H., Burke, A. P., Kamm, R. D., Lee, R. T., 2001. The impact of calcification on the biomechanical stability of atherosclerotic plaques. *Circulation* 103, 1051–1056.

[31] Humphrey, J. D., 2002. Continuum biomechanics of soft biological tissues. *Proceedings of the Royal Society A: Mathematical, Physical and Engineering Sciences* 175, 1–44.

[32] Jaroslav, V., Jiri, S., Dita, V., Karel, V., 1999. Residual strain in human atherosclerotic coronary arteries and age related geometrical changes. *Bio- Medical Materials and Engineering* 9, 311–317.

[33] Kips, J. G., Segers, P., Van Bortel, L. M., 2008. Identifying the vulnerable plaque: A review of invasive and non-invasive imaging modalities. *Artery Research* 2, 21–34.

[34] Kock, S. A., Nygaard, J. V., Eldrup, N., Fründ, E.-T., Klærke, A., Paaske, W. P., Falk, E., Kim, W. Y., 2008. Mechanical stresses in carotid plaques using mri-based fluid-structure interaction models. *Journal of Biomechanics* 41, 1651 – 1658.

[35] Krishna Kumar, R., Balakrishnan, K. R., 2005. Influence of lumen shape and vessel geometry on plaque stresses: possible role in the increased vulnerability of a remodelled vessel and the shoulder of a plaque. *Heart* 91, 1459–1465.

[36] Kyriacou, S., Schwab, C., Humphrey, J., 1996. Finite element analysis of non-linear orthotropic hyperelastic membranes. *Computational Mechanics* 18, 269–278.

[37] Lee, R., 2000. Atherosclerotic lesion mechanisc versus biology. *Zeitschrift fur Kardiologie* 89, 80–84.

[38] Lee, R., Loree, H., Cheng, G., Lieberman, E., Jaramillo, N., Schoen, F., 1993. Computational structural analysis based on intravascular ultrasound imaging before in vitro angioplasty: Prediction of plaque fracture locations. *Journal of the American College of Cardiology* 21, 777–782.

[39] Lendon, C. L., Davies, M., Born, G., Richardson, P., 1991. Atherosclerotic plaque caps are locally weakened when macrophages density is increased. *Atherosclerosis* 87, 87–90.

[40] Lloyd-Jones, D., Adams, R., Carnethon, M., De Simone, G., Ferguson, T. B., Flegal, K., Ford, E., Furie, K., Go, A., Greenlund, K., Haase, N., Hailpern, S., Ho, M., Howard, V., Kissela, B., Kittner, S., Lackland, D., Lisabeth, L., Marelli, A., McDermott, M., Meigs, J., Mozaffarian, D., Nichol, G., O'Donnell, C., Roger, V., Rosamond, W., Sacco, R., Sorlie, P., Stafford, R., Steinberger, J., Thom, T., Wasserthiel-Smoller, S., Wong, N., Wylie-Rosett, J., Hong, Y., for the American Heart Association Statistics Committee, Subcommittee, S. S., 2009. Heart disease and stroke statistics–2009 update: A report from the american heart association statistics committee and stroke statistics subcommittee. *Circulation* 119, 21–181.

[41] Loree, H., Kamm, R., Stringfellow, R., Lee, R., 1992. Effects of fibrous cap thickness on peak circumferential stress in model atherosclerotic vessels. *Circulation Research* 71, 850–858.

[42] Loree, H. M., Grodzinsky, A. J., Park, S. Y., Gibson, L. J., Lee, R. T., 1994. Static circumferential tangential modulus of human atherosclerotic tissue. *Journal of Biomechanics* 27, 195–204.

[43] Marquardt, D. W., 1963. An algorithm for least-squares estimation of nonlinear parameters. *SIAM Journal on Applied Mathematics* 11, 431–441.

[44] Mathers, C., Murray, C., 2006. Global burden of disease and risk factors, chapter the burden of disease and mortality by condition: Data, methods, and results for 2001. Oxford University Press , 45–240.

[45] Moreno, P. R., Purushothaman, K. R., Fuster, V., O'Connor, W. N., 2002. Intimo-medial interface damage and adventitial inflammation is increased beneath disrupted atherosclerosis in the aorta: Implications for plaque vulnerability. *Circulation* 105, 2504–2511.

[46] Naghavi, M., Libby, P., Falk, E., Casscells, S. W., Litovsky, S., Rumberger, J., Badimon, J. J., Stefanadis, C., Moreno, P., Pasterkamp, G., Fayad, Z., Stone, P. H., Waxman, S., Raggi, P., Madjid, M., Zarrabi, A., Burke, A., Yuan, C., Fitzgerald, P. J., Siscovick, D. S., de Korte, C. L., Aikawa, M., Juhani Airaksinen, K., Assmann, G., Becker, C. R., Chesebro, J. H., Farb, A., Galis, Z. S., Jackson, C., Jang, I.-K., Koenig, W., Lodder, R. A., March, K., Demirovic, J., Navab, M., Priori, S. G., Rekhter, M. D., Bahr, R., Grundy, S. M., Mehran, R., Colombo, A., Boerwinkle, E., Ballantyne, C., Insull, William, J., Schwartz, R. S., Vogel, R., Serruys, P. W., Hansson, G. K., Faxon, D. P., Kaul, S., Drexler, H., Greenland, P., Muller, J. E., Virmani, R., Ridker, P. M., Zipes, D. P., Shah, P. K., Willerson, J. T., 2003. From vulnerable plaque to vulnerable patient: A call for new definitions and risk assessment strategies: Part I. *Circulation* 108, 1664–1672.

[47] Ohayon, J., Dubreuil, O., Tracqui, P., Le Floc'h, S., Rioufol, G., Chalabreysse, L., Thivolet, F., Pettigrew, R. I., Finet, G., 2007. Influence of residual stress/strain

on the biomechanical stability of vulnerable coronary plaques: potential impact for evaluating the risk of plaque rupture. *American Journal of Physiology - Heart* 293, H1987–H1996.

[48] Ohayon, J., Finet, G., Gharib, A. M., Herzka, D. A., Tracqui, P., Heroux, J., Rioufol, G., Kotys, M. S., Elagha, A., Pettigrew, R. I., 2008. Necrotic core thickness and positive arterial remodeling index: emergent biomechanical factors for evaluating the risk of plaque rupture. *American Journal of Physiology - Heart* 295, H717–H727.

[49] Ohayon, J., Finet, G., Treyve, F., Rioufol, G., Dubreuil, O., 2005. A three dimensional finite element analysis of stress distribution in a coronary atherosclerotic plaque: In-vivo prediction of plaque rupture location. *Biomechanics Applied to Computer Assisted Surgery* 17, 225–241.

[50] Ohayon, J., Teppaz, P., Finet, G., Rioufol, G., 2001. In-vivo prediction of human coronary plaque rupture location using intravascular and finite element method. *Coronary Artery Disease* 12, 655–663.

[51] Pasterkamp, G., de Kleijn, D. P., Borst, C., 2000. Arterial remodeling in atherosclerosis, restenosis and after alteration of blood flow: potential mechanisms and clinical implications. *Cardiovascular Researcher* 45, 843–852.

[52] Peña, E., Alastraúé, V., Laborda, A., Martínez, M., Doblaré, M., 2010. A constitutive formulation of vascular tissue mechanics including viscoelasticity and softening behaviour. *Journal of Biomechanics* 43, 984–989.

[53] Peña, E., del Palomar, A. P., Calvo, B., Martínez, M. A., Doblaré, M., 2007. Computational modelling of diarthrodial joints. Physiological, pathological and pos-surgery simulations. *Archives of Computational Methods in Engineering* 14(1), 47–91.

[54] Roger, V. L., Go, A. S., Lloyd-Jones, D. M., Adams, R. J., Berry, J. D., Brown, T. M., Carnethon, M. R., Dai, S., de Simone, G., Ford, E. S., Fox, C. S., Fullerton, H. J., Gillespie, C., Greenlund, K. J., Hailpern, S. M., Heit, J. A., Ho, P. M., Howard, V. J., Kissela, B. M., Kittner, S. J., Lackland, D. T., Lichtman, J. H., Lisabeth, L. D., Makuc, D. M., Marcus, G. M., Marelli, A., Matchar, D. B., McDermott, M. M., Meigs, J. B., Moy, C. S., Mozaffarian, D., Mussolino, M. E., Nichol, G., Paynter, N. P., Rosamond, W. D., Sorlie, P. D., Stafford, R. S., Turan, T. N., Turner, M. B., Wong, N. D., Wylie-Rosett, J., 2011. Heart disease and stroke statistics - 2011 update. *Circulation* 123 (4), e18–e209.

[55] Salunke, N. V., Topoleski, L. D. T., Humphrey, J. D., Mergner, W. J., 2001. Compressive stress-relaxation of human atherosclerotic plaque. *Journal of Biomedical Materials Research Part A* 55, 236–241.

[56] Simo, J. C., 1991. Algorithms for Static and Dynamic Multiplicative Plasticity that Preserve the Classical Return Mapping Schemes of the Infinitesimal Theory. *Computer Methods in Applied Mechanics and Engineering* 99, 61–112.

[57] Smedby, O., 1998. Geometrical risk factors for atherosclerosis in the femoral artery: A longitudinal angiographic study. *Annals of Biomedical Engineering* 26, 391–397.

[58] Spencer, A. J. M., 1971. Theory of invariants. In: *Continuum Physics*. Academic Press, New York, pp. 239–253.

[59] Tang, D., Teng, Z., Canton, G., Yang, C., Ferguson, M., Huang, X., Zheng, J., Woodard, P. K., Yuan, C., 2009. Sites of rupture in human atherosclerotic carotid plaques are associated with high structural stresses: An in vivo MRI-based 3D fluid-structure interaction study. *Stroke* 40, 3258–3263.

[60] Tang, D., Yang, C., Zheng, J., Woodard, P., Saffitz, J., Petruccelli, J., Sicard, G., Yuan, C., 2005. Local maximal stress hypothesis and computational plaque vulnerability index for atherosclerotic plaque assessment. *Annals of Biomedical Engineering* 33, 1789–1801.

[61] Tang, T., Howarth, S., Li, Z., Miller, S., Graves, M., U-King-Im, J., Trivedi, R., Walsh, S., Brown, A., Kirkpatrick, P., Gaunt, M., Gillard, J., 2008. Correlation of carotid atheromatous plaque inflammation with biomechanical stress: Utility of USPIO enhanced MR imaging and finite element analysis. *Atherosclerosis* 196, 879 – 887.

[62] Thubrikar, M., 2007. *Vascular mechanics and pathology*. Springer Science.

[63] Van der Wal, A. C., Becker, A. E., 1999. Atherosclerotic plaque rupture - pathologic basis of plaque stability and instability. *Cardiovascular Research* 41, 334–344.

[64] VanEpps, J. S., Vorp, D. A., 2007. Mechanopathobiology of atherogenesis: A review. *Journal of Surgical Research* 142, 202–217.

[65] Varnava, A. M., Mills, P. G., Davies, M. J., 2002. Relationship between coronary artery remodeling and plaque vulnerability. *Circulation* 105, 939–943.

[66] Vengrenyuk, Y., Carlier, S., Xanthos, S., Cardoso, L., Ganatos, P., Virmani, R., Einav, S., Gilchrist, L., Weinbaum, S., 2006. A hypothesis for vulnerable plaque rupture due to stress-induced debonding around cellular microcalcifications in thin fibrous caps. *Proceedings of the National Academy of Sciences* 103, 14678–14683.

[67] Versluis, A., Bank, A. J., Douglas, W. H., 2006. Fatigue and plaque rupture in myocardial infarction. *Journal of Biomechanics* 39, 339–347.

[68] Virmani, R., Burke, A. P., Farb, A., Kolodgie, F. D., 2006. Pathology of the vulnerable plaque. *Journal of the American College of Cardiology* 47, C13–18.

[69] Virmani, R., Kolodgie, F. D., Burke, A. P., Farb, A., Schwartz, S. M., 2000. Lessons from sudden coronary death: A comprehensive morphological classification scheme for atherosclerotic lesions. *Arteriosclerosis, Thrombosis, and Vascular Biology* 20, 1262–1275.

[70] Weiss, J. A., 1994. A constitutive model and finite element representation for transversely isotropic soft tissues. Ph.D. thesis, The University of Utah.

[71] Wenk, J. F., 2011. Numerical modeling of stress in stenotic arteries with microcalcifications: A parameter sensitivity study. *ASME Journal of Biomechanical Engineering* 133, 014503.

[72] Williamson, S. D., Lam, Y., Younis, H. F., Huang, H., Patel, S., Kaazempur-Mofrad, M. R., Kamm, R. D., 2003. On the sensitivity of wall stresses in diseased arteries to variable material properties. *ASME Journal of Biomechanical Engineering* 125, 147–155.